

A Humanized Yeast Platform for Functional Characterization of TRAPP Complex Variants Linked to Rare Disease

Chelsea Abboud

A Thesis

In the Department of Biology

Presented in Partial Fulfillment of the Requirements for the Degree of Master of Science
(Biology)

Concordia University, Montréal, Quebec

August, 2025

© Chelsea Abboud

CONCORDIA UNIVERSITY
School of Graduate Studies

This is to certify that the thesis prepared

By: Chelsea Abboud

Entitled: A Humanized Yeast Platform for Functional Characterization of TRAPP Complex Variants Linked to Rare Disease

and submitted in partial fulfillment of the requirements for the degree of

Master of Science (Biology)

complies with the regulations of the University and meets the accepted standards with respect to originality and quality.

Signed by the final examining committee:

Dr. Michael Sacher _____ Chair

Dr. William Zerges _____ Examiner

Dr. Malcolm Whiteway _____ Examiner

Dr. Isabelle Gelber _____ External Examiner

Dr. Michael Sacher _____ Thesis Supervisor(s)

Approved by Dr. Robert Weladji _____
Chair of Department or Graduate Program Director

Dr. Pascale Sicotte Dean of Faculty of Arts and Science

Abstract:

A Humanized Yeast Platform for Functional Characterization of TRAPP Complex Variants in Rare Disease

Chelsea Abboud, MSc

The Transport Protein Particle (TRAPP) complex is a highly conserved multi-subunit tethering complex that plays a critical role in membrane trafficking. Mutations in TRAPP complex subunits have been implicated in a growing spectrum of rare genetic disorders, yet the molecular mechanisms underlying variant pathogenicity often remain unclear. In this thesis, I developed a humanized yeast platform to enable systematic functional characterization of TRAPP complex variants of unknown significance. Using a stepwise gene replacement strategy in *Saccharomyces cerevisiae*, I reconstructed the core TRAPP complex with human orthologs, and constructed a strain containing five of the human subunits. The integration of human subunits was validated through RT-PCR and Western blotting. Growth assays revealed that partial humanization of the core complex recapitulates key functional aspects of TRAPP assembly and enables the investigation of disease-associated variants *in vivo*. Structural modeling and clash analysis using PyMOL provided insights into the impact of specific mutations on complex stability and subunit interactions. Introduction of a clinically relevant C3 (L131F) variant into the humanized strain resulted in pronounced growth defects and predicted structural clashes, supporting its pathogenicity. This work demonstrates the power of humanized yeast as a model for elucidating genotype-phenotype relationships in rare TRAPPopathies, and provides a versatile platform for variant interpretation, mechanistic studies, and potential therapeutic screening.

Acknowledgments

To my PI, Dr. Sacher: Thank you for giving me a chance when I was an international student and a fresh graduate whom you didn't know anything about. I am incredibly grateful for the trust you placed in me, for all that you have taught me, and for the opportunities your mentorship has opened for me. You have shaped me as a researcher, and your dedication, humility, positivity, and genuine love for your work have truly inspired me. Thank you for always encouraging me to give more, for holding me accountable, and for believing in me. I have grown not only as a scientist but also as a person because of my time in your lab.

To my parents, Aline and Youssef: No words could ever express how grateful I am to have you in my life. I have never known a love as pure and unconditional as yours. Without you, I am nothing. Thank you for always putting my needs above your own, for your wise advice, and for encouraging me to never settle, always aim higher, and take risks. Your sacrifices and unwavering belief in me have carried me through every challenge, and I dedicate this accomplishment to you both.

To my older sisters, Gaelle and Carel: Thank you for always worrying about me, for giving me advice, and for trying to guide me, even when I did not always listen. I used to get annoyed when you called me "baby sister," but now I understand that this is just your way of showing love. No matter how old I get, I know I will always be your little sister, and I am grateful for your encouragement and support throughout this journey.

To my partner Chris, the calm in the middle of the storm. When I am with you, I am the best version of myself, and for that, I am forever grateful. Thank you for all the times you challenged me and for all the questions you asked that pushed me to think more deeply. Thank you for always picking up the pieces when I am down and for being the shoulder I can lean on. Thank you for celebrating my successes, cheering me on through setbacks, and reminding me to keep going. I am so grateful that you are not only my partner, but also my best friend.

To my committee member and course instructor, Dr. Zerges, I never imagined I could learn so much in just two semesters. Thank you not only for being my teacher but also for all the times you welcomed me into your office to offer advice and guidance. You have truly taught me how to think like a researcher. To Dr. Whiteway, thank you for agreeing to serve on my committee and for contributing such valuable insights during my committee meetings.

To my lab mates Aaliya, Rozmehr, and Mahsa, thank you for being like older sisters to me in the lab. We have fought, celebrated, and cried together just like family. You truly made coming to the lab enjoyable, even on the most stressful days. I am grateful for every time you listened to me and for all our science talks, from which I learned so much. Whether we were troubleshooting experiments late at night or sharing a laugh after a long day, your support meant everything. Hearing about your experiences in the field was always inspiring, and I hope we will stay in touch even after I leave.

To the friends I made at Concordia, thank you for your kindness and support throughout my studies. You made my experience here truly memorable and enjoyable.

Contribution of Authors:

Table 2.4, 2.6, 2.7 – Primers and sgRNA were prepared by Britanny Gecco

Figure 3.5 (A-B) and Figure (3.9) – Rozmehr Shokohi performed the RT-PCR experiments for C2L, C6B, and C4ΔPDZL.

Figure 3.14C – Aaliya Naaz contributed to the validation of the liquid growth curve at 37 °C by independently conducting the third experimental replicate.

Figure 3.18A – Aaliya Naaz performed the liquid growth curve assays at 25 °C for the parental strain, C3 (WT), and C3 (L131F).

Table of Contents

1	<i>Introduction</i>	1
1.1	Why study rare disease?.....	1
1.2	Model organisms in rare disease research.....	1
1.2.1	Overview and Advantages of Model Organisms	1
1.2.2	Yeast as a model organism of choice:.....	2
1.3	Humanization in yeast.....	2
1.3.1	Functional Humanization of Yeast Genes and Complexes.....	2
1.4	Variants of Unknown Significance.....	4
1.4.1	Definition of Variants of Unknown Significance (VUS) and Clinical Relevance.....	4
1.4.2	Classic and new approaches for studying VUS	4
1.4.3	Humanized Yeast to study VUS.....	5
1.5	The TRAPP complex	6
1.5.1	Introduction to TRAPP.....	6
1.5.2	TRAPP Complexes in Yeast.....	6
1.5.3	TRAPP Complexes in Humans:.....	8
1.5.4	Function of the TRAPP complexes in Humans	9
1.5.5	Orthology between yeast and human TRAPP core subunits.....	9
1.5.6	Yeast Trapp Core Subunit Organization	10
1.5.7	TRAPP-associated disorders (TRAPPopathies).....	11
1.6	Previous Work and Objective.....	15
1.6.1	Previous work on the humanized model	15
1.6.2	Objectives.....	15
2	<i>Materials and Methods:</i>	16
2.1	Plasmids, Strains, and Media.....	16
2.1.1	Plasmids and Yeast strains used in the study:.....	16

2.1.2	Media used in this study.....	17
2.2	Yeast Transformation and Humanization Protocol	18
2.2.1	Humanization Using Frozen-EZ Yeast Transformation	18
2.2.2	Standard Lithium Acetate Yeast transformation.....	19
2.2.3	Bacterial Transformation for Plasmid Propagation.....	19
2.3	Genomic DNA preparation and confirmation	20
2.3.1	Genomic DNA extraction from yeast cells	20
2.3.2	Confirmation PCR:.....	21
2.3.3	Sequencing of Humanized Genes	21
2.4	sgRNA Design Cloning.....	22
2.4.1	sgRNA Design and Validation.....	22
2.4.2	Golden Gate Assembly for sgRNA cloning.....	23
2.5	Functional Assays and Expression Analysis.....	24
2.5.1	Liquid growth curve yeast assay.....	24
2.5.2	Spot Dilution Assay	25
2.5.3	Western blot yeast lysates	25
2.5.4	Invertase Assay	26
2.5.5	Gene expression using RT-PCR.....	27
2.6	Structural Analysis	28
2.6.1	Structural Clash Analysis (Pymol).....	28
2.6.2	Strctrual clash analysis (ChimeraX).....	28
3	Results:	30
3.1	Humanization and validation of the replacement TRAPP core subunits <i>C1</i>, <i>C2L</i>, and <i>C6B</i>.....	30
3.2	Humanization of <i>C4</i> and <i>C3</i> subunits and unsuccessful restoration of the PDZL domain	35
3.3	<i>C2</i> and <i>C5</i> could not replace their orthologues <i>TRS20</i> and <i>TRS31</i> in the PHTCC strain	43
3.4	Structural modeling and clash analysis of PHTCC.....	44

3.5	Sequential humanization of <i>C2</i>.....	47
3.6	Functional assessment of humanized strains by growth curve analysis	49
3.7	Structural mapping and effects of <i>C3 L131F</i> mutant.....	52
3.8	Successful humanization of the L131F mutant.....	54
3.9	Characterization of the <i>L131F C3</i> mutant	55
4	<i>Discussion and future work:</i>.....	60
5	<i>References:</i>.....	69

List of Figures

Figure 1.1 Cryo-EM structure of the yeast TRAPP core (PDB: 7E2D).....	7
Figure 1.2 Predicted arrangement of the human TRAPP core subunits.	8
Figure 1.3 Structure summary and associated disorder with each subunit	14
Figure 3.1 CRISPR-Cas9-mediated humanization of TRAPP complex subunits in yeast.....	31
Figure 3.2 Confirmation PCR of all human subunits.....	32
Figure 3.3 Sanger Sequencing of C1, C2L, and C6B.	33
Figure 3.4 Real Time PCR showing expression of C2L, C4ΔPDZL, and C6B..	34
Figure 3.5 Successful humanization of C4ΔPDZL.....	36
Figure 3.6 Successful humanization of C3.	37
Figure 3.7 Verification of successful C4ΔPDZL and C3 scarless replacement via Sanger sequencing.....	38
Figure 3.8 Western blots showing expression of the humanized C3 and C4ΔPDZL subunits....	39
Figure 3.9 Real Time PCR for C4ΔPDZL in PHTCC.....	40
Figure 3.10 Attempted replacement of human C4ΔPDZL with full-length C4 ORF.	41
Figure 3.11 Clashes of C4ΔPDZL vs C4 in PHTCC.....	42
Figure 3.12 CRISPR-Cas9-mediated humanization of C5 and C2 in a PHTCC background.	44
Figure 3.13 Sequential humanization of the TRAPP core reveals emergence of subunit-specific steric clashes by structural modeling..	47
Figure 3.14 Sequential humanization of the C2 Subunit across intermediate humanized TRAPP strain backgrounds using CRISPR-Cas9.....	48
Figure 3.15 Temperature-dependent growth analysis of sequentially humanized TRAPP core strains.	51
Figure 3.16 Structural and sequence analysis of the C3 L131F mutant and its effects on protein packing.	53

Figure 3.17 Successful humanization of the L131F in the PHTCC.....	54
Figure 3.18 Sanger sequencing confirmation of <i>C3 L131F</i> mutation in the humanized yeast strain	55
Figure 3.19 Growth analysis of parental, C3 wild-type, and C3 (L131F) mutant strains at different temperatures.....	57
Figure 3.20 Secretion assay to characterize C3 L131F mutant... ..	59
Figure 4.1 C5 and Trs31 Overlay.	64
Figure 4.2 Graphical abstract showing significance of study	67

List of Tables

Table 1.1 Yeast and human TRAPP core subunit orthologues, essentiality, and sequence conservation.....	10
Table 1.2 Clinical and cellular consequences of mutations in TRAPP subunits.....	13
Table 2.1 Plasmids used in this study.....	16
Table 2.2 Yeast strains used in this study	17
Table 2.3 Transformation conditions and concentrations.	18
Table 2.4 Confirmation PCR primers list.....	21
Table 2.5 PCR set up.....	21
Table 2.6 List of primers used for sequencing.....	22
Table 2.7 List of sgRNA targeting the genes in yeast	23
Table 2.8 Real-Time PCR components	27
Table 2.9 Real-Time PCR primers	27

List of Abbreviations:

CRISPR	Clustered Regularly Interspaced Short Palindromic Repeats
DSB	Double Stranded Breaks
ER	Endoplasmic Reticulum
GEF	Guanine Nucleotide Exchange Factor
HDR	Homology Directed Repair
NGS	Next Generation Sequencing
ORF	Open Reading Frame
SMS	Saccharomycotina-specific domain
sgRNA	Single guide RNA
SEDT	Spondyloepiphyseal Dysplasia Tarda
TRAPP	Transport Protein Particle
VUS	Variants of Unknown Significance
UTR	Untranslated Region
PHTC	Partially Humanized TRAPP Complex

1 Introduction

1.1 The importance of studying rare diseases

When looking at individual cases, rare diseases are uncommon. However, when taken together, it is estimated that 300 million people worldwide are affected by some form of a rare disease (Somanadhan et al., 2020). Patients often endure a lifelong “diagnostic odyssey”, lasting an average of 6 years before receiving an accurate diagnosis. This delay often imposes profound impacts in terms of chronic, severe, and life-threatening symptoms in some patients. The delay is due to several reasons including heterogeneity of symptoms, low clinical awareness, and limited research data for each condition.

The study of rare diseases is not only impactful to improve diagnostics, finding cures, and treatments, but it also has the potential to advance general medical knowledge through the study of fundamental biological processes that are relevant to more common conditions (Baldridge et al., 2021). One way that could happen is through the identification of the genetic cause of a rare disorder which can reveal new pathways/mechanisms that might be targeted in common diseases (Baldridge et al., 2021). However, since patient numbers are low, and procedures to acquire patient cells are invasive, studying rare diseases in human populations is difficult. This is where model organisms are essential.

1.2 Model organisms in rare disease research.

1.2.1 Overview and Advantages of Model Organisms

Model organisms which include yeast, worms, flies, and fish have proven useful in studying rare disease, specifically for providing the platform for functional studies for genetic disease, and the development of new therapeutic strategies (Wangler et al., 2017). Many human genes linked to rare disease have orthologues in model organisms. This enables researchers to recreate the disease-causing mutations in an experimental setting. Moreover, model systems offer advantages such as easy genetic manipulation,

fast generation times, and controlled environments, which make it feasible to dissect the cellular effects of a mutation (Fields & Johnston, 2005).

1.2.2 Yeast as a model organism of choice:

Yeast (*Saccharomyces cerevisiae*) is an invaluable tool for revealing human cellular pathways and disease (Laurent et al., 2016). In contrast to using a human cell line or animal model, making a custom genetic variant in yeast is inexpensive and simple. Yeast is characterized by a fast-doubling time allowing for high throughput experiments and selection screens that would otherwise be impractical in mammals. Moreover, through the use of yeast, entire gene products have been assigned to genes solely through genetics. This would have been impossible using a biochemical approach. For example, genes whose products are involved in secretion have been identified through a genetic screen for temperature sensitive mutants that accumulated secretory proteins at a non-permissive temperature (Kaiser & Schekman, 1990). These features establish yeast as a powerful platform for modeling human gene function and dissecting conserved cellular processes.

1.3 Humanization in yeast

1.3.1 Functional Humanization of Yeast Genes and Complexes

Despite being a single celled fungus, human genes are widely conserved in yeast (Kachroo et al., 2015). This means that human genes can potentially replace their yeast orthologues, allowing a platform to study human genes.. Due to ease of genetic manipulation of yeast, one can readily delete, insert, or modify the genes of interest. This is possible due to the advent of CRISPR/CAS9 technology and the fact that yeast tend to adopt homology directed repair (HDR). These components allow one to edit yeast in a scarless way meaning just targeting the start codon to stop codon. “Humanization” refers to modification of a

model organism in a way that it expresses the orthologous human open reading frame (ORF) instead of its own (Kachroo et al., 2022). The goal is for the yeast cell to rely on the human gene to perform a cellular function (Laurent et al., 2016).

A classical use is to test for functional complementation where one tests whether the human ORF can replace the function of the yeast gene (Hamza et al., 2015). This was demonstrated when the human *RAS* gene was expressed in yeast proving to complement the yeast *RAS* gene, in a *ras* knockout (Kataoka et al., 1985). Since then, hundreds of human genes, with focus on essential genes, have been successfully humanized in yeast. A seminal study that replaced 414 yeast genes with their human orthologues one by one, demonstrated that 47% of the human genes (essential in yeast) could complement their yeast orthologue (Kachroo et al., 2022). This shows that there is a significant amount of gene functions that could be interchangeable even after millions of years of evolution. It is worth noting that humanization does not have to be limited to single genes. There are five degrees of yeast humanization: assays on yeast to study human disease, heterologous expression of human genes, humanizing specific sites, humanizing entire genes, and even humanizing full pathways (Laurent et al., 2016). In fact, the humanization of the glycolysis pathway in yeast has been possible through the replacement of 10 human enzymes in yeast (Boonekamp et al., 2022). This generated a yeast strain that was able to carry out glycolysis using the complete set of human enzymes, although certain enzymes required adaptive mutations to achieve optimal functionality in the yeast cellular environment. There is numerous evidence indicating that humanization of complexes is possible. One example is the human proteasome complex which breaks down proteins in the cell that are no longer needed. Nearly all human proteasome subunits were replaceable except for a couple which was due to species specific protein interaction (Sultana et al., 2023). Another example is the humanization of the kinetochore, whereby the replacement of *Cse4* with human CENP-A was possible due to the humanization of partner proteins. Thus, investigators were able to create a hybrid kinetochore to study human chromatin behavior in yeast cells (Olafsson et al., 2023). These examples show that the humanization of yeast is indeed achievable and useful. However, it is

worth noting that the humanization of some yeast genes might need additional modification or multiple gene replacement for full functionality. Humanization often reveals protein-protein interaction specificity. If a protein fails to function/complement its yeast homologue it might indicate that it cannot interact with a neighboring yeast partner.

1.4 Variants of Unknown Significance

1.4.1 Definition of Variants of Unknown Significance (VUS) and Clinical Relevance

VUS are genetic modifications that have been identified through sequencing, but their clinical significance has not yet been established (Timmermans, 2017). These variants are more prominent in rare diseases as there are many fewer patients which limits the interpretation of genetic results. This ambiguity might prevent or delay a timely diagnosis. Therefore, a rapid method is needed to characterize the VUS pathogenicity.

1.4.2 Classic and new approaches for studying VUS

The methods to categorize VUS can be broadly characterized into classical and emerging approaches to study rare disease. The classical approaches refer to methods that have been established and used for many years to study VUS, whereas the emerging approaches leverage recent advances in genomics to allow for systematic variant assessment.

Classical methods for assessing variants of unknown significance span computational, cellular, organismal, and patient-derived systems. In silico prediction tools, which analyze structural features, offer a fast and accessible means to prioritize variants by estimating their potential effects. However, these predictions remain speculative without experimental validation, as they may not account for complex cellular contexts (Cannon et al., 2023). *In vitro* functional assays provide cellular-level insights by expressing mutant proteins in model cell lines. These assays are valuable for characterizing biochemical activity, subcellular localization, and protein–protein interactions, though they can be

laborious and resource-intensive (Kimura et al., 2022). At the organismal level, *in vivo* animal models allow researchers to observe variant-induced phenotypes. While offering high biological relevance, such models are limited by ethical considerations, cost, and low throughput (Twigg et al., 2025). Finally, patient-derived cell analyses leverage primary cells from individuals carrying the variant, capturing physiologically relevant effects. Yet, their use is constrained by the invasiveness of sample collection and limited availability, especially for rare diseases (Wu et al., 2022).

Emerging approaches offer new ways to study rare disease to address the limitations of classical methods. One such approach involves humanized model organisms, where endogenous genes in model organisms are replaced with human orthologs (either wild-type or mutant forms) to assess variant function *in vivo*. This method allows scalable and functionally relevant experimentation but requires careful design, as not all human genes have direct counterparts in model organisms (Kachroo et al., 2022). Another powerful technique is site saturation mutagenesis (SSM), which introduces all possible single-nucleotide variants into a gene to map critical residues. When used in humanized yeast, for instance, SSM enables systematic high throughput classification of variants. It is worth noting that it remains best suited for genes with clear, selectable phenotypes (Abt et al., 2016). Additionally, Next Generation Sequencing (NGS)-based transcriptomic assays (including RNA-seq and targeted splicing analyses) have become indispensable for detecting variant-induced disruptions in gene expression and splicing. While these high-throughput techniques offer sensitivity and resolution across thousands of variants, they also demand extensive computational resources and expertise for accurate interpretation (Satam et al., 2023).

1.4.3 Humanized Yeast to study VUS

In the context of rare diseases, patient-derived cells are often not readily available, making timely functional validation of VUS particularly challenging. A humanized yeast model offers a powerful alternative for rapidly characterizing disease-causing mutations. As highlighted above, combining

emerging methods such as saturation mutagenesis and next-generation sequencing (NGS) with a humanized model organism enables high-throughput functional screening of large variant libraries. This approach provides a direct link between genotype and phenotype, facilitating the interpretation of VUS in a clinically relevant timeframe even when patient samples are unavailable.

1.5 The TRAPP complex

1.5.1 Introduction to TRAPP

The Transport Protein Particle (TRAPP) complex is a multi-subunit complex that is highly conserved and functions in intracellular vesicle trafficking (Sacher et al., 1998). It was initially identified in yeast and shown to function in endoplasmic reticulum (ER) to Golgi transport. Later, it was shown to act as a guanine nucleotide exchange factor (GEF) for Ypt/Rab GTPases (Morozova et al., 2006; Wang et al., 2000). GEFs catalyze GDP to GTP exchange on specific Rab proteins, ensuring that Rabs are activated at the correct time and location, thereby ensuring proper vesicle targeting and fusion.

1.5.2 TRAPP Complexes in Yeast.

The TRAPP complexes were first identified in yeast, and shown to have three related complexes called TRAPPI, TRAPPII, and TRAPPIII (Lynch-Day et al., 2010; Sacher & Ferro-Novick, 2001). All three share a common core of subunits (**Figure 1.1**) but include distinct accessory subunits that tailor each complex to a specific pathway. However, TRAPPI is considered to be an *in vitro* artifact since it only is seen in organisms with a *Saccharomycotina*-specific domain (SMS) present on the Trs23p subunit (Brunet et al., 2012). In addition, *in vivo* work suggests the presence of only TRAPPII and III (Thomas & Fromme, 2016; Thomas et al., 2018). For these reasons, TRAPPI appears to be an *in vitro* artifact representing the common core of TRAPPII and TRAPPIII (Brunet et al., 2012). The TRAPP core is composed of Bet3p (two copies), Bet5p, Trs20p, Trs23p Trs31p, and Trs33p (Sacher et al., 1998).

TRAPPII has additional subunits called Trs65p, Trs120p, Trs130p and Tca17p (Choi et al., 2011; Sacher et al., 2001; Scrivens et al., 2009), while TRAPPIII is composed of the core with an additional subunit Trs85 (Lynch-Day et al., 2010).

The TRAPP subunits that are essential for yeast cell viability are Bet3p, Bet5p, Trs20p, Trs23p, Trs31p, Trs120p, and Trs130p, while Trs33p, Trs65p, and Trs85p are non-essential under standard growth conditions (Kim et al., 2016; Tokarev et al., 2009).

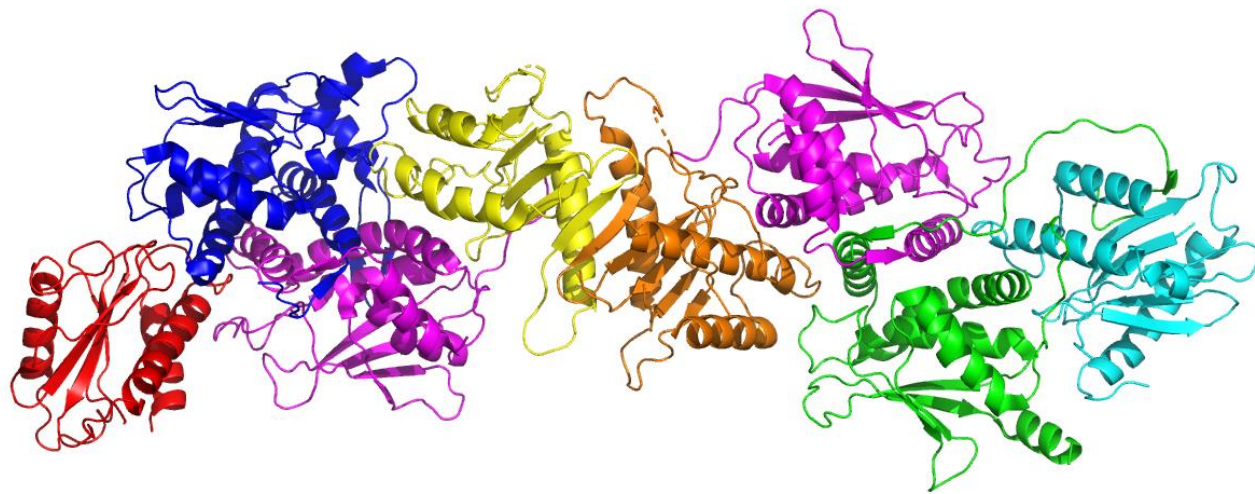


Figure 1.1 Cryo-EM structure of the yeast TRAPP core (PDB: 7E2D). The structure of the yeast TRAPP core complex is shown, derived from the cryo-electron microscopy (cryo-EM) structure of the TRAPPII complex (PDB: 7E2D; Sui et al., 2022). TRAPPII-specific subunits were removed in silico to highlight the core subunits only. Each core subunit is colored by chain: Tca17 (chain A, red), Trs33 (chain B, blue), Bet3 (chains C and F, magenta), Bet5 (chain D, yellow), Trs23 (chain E, orange), Trs31 (chain G, green), and Trs20 (chain H, cyan). Visualization and coloring were performed in PyMOL. The structure demonstrates the conserved architecture of the TRAPP core.

1.5.3 TRAPP Complexes in Humans:

The TRAPP complex was identified in both yeast and humans in early proteomic studies, which revealed a highly conserved subunit composition across species (**Table 1.1**) (Gavin et al., 2002; Sacher et al., 2001). Two TRAPP complexes are recognized in humans: TRAPPII and TRAPPIII (Choi et al., 2011; Riedel et al., 2018). Both of these complexes share a conserved common core of subunits (TRAPPC1, TRAPPC2, TRAPPC2L, TRAPPC3, TRAPPC4, TRAPPC5, and TRAPPC6A/B) (**Figure 1.2**) (Riedel et al., 2018). TRAPPII incorporates two additional subunits, TRAPPC9 and TRAPPC10, while TRAPPIII includes four unique subunits: TRAPPC8, TRAPPC11, TRAPPC12, and TRAPPC13 (Lynch-Day et al., 2010; Shirahama-Noda et al., 2013).

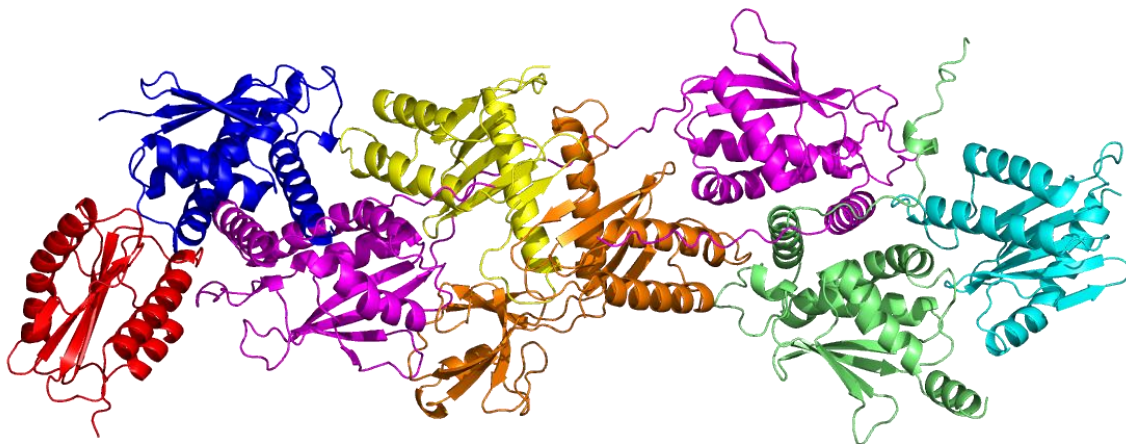


Figure 1.2 Predicted quaternary structure of the human TRAPP core subunits. The structure shown represents the predicted arrangement of the human TRAPP core complex, visualized using PyMOL. Individual subunits were predicted using AlphaFold and subsequently aligned to their corresponding yeast counterparts based on the 7E2D structure, using the PyMOL command align TrappC#, 7E2D and chain [Letter]. The align command works optimally when the proteins are homologous and share similar sequence and residue numbering, matching residues by number and atom name to minimize the RMSD between structures. For clarity, each human subunit was assigned a distinct color: TRAPPC2L (red), TRAPPC6B (blue), TRAPPC1 (yellow), TRAPPC3 (magenta), TRAPPC4 (orange), TRAPPC5 (green), and TRAPPC2 (cyan).

1.5.4 Function of the TRAPP complexes in Humans

In mammalian cells, the TRAPP complexes play distinct roles in regulating membrane trafficking pathways through specific interactions with Rab GTPases. TRAPPII has been implicated in the regulation of Rab11-dependent trafficking, particularly through its role in facilitating the delivery of Rabin8, a GEF for Rab8, to the centrosome (Westlake et al., 2011). This TRAPPII- and Rab11-dependent trafficking step is essential for primary ciliogenesis, the process by which cells assemble specialized, hair-like cilia that play key sensory and signaling roles. While the direct GEF activity of TRAPPII towards Rab11 in human cells has yet to be firmly established, studies in yeast demonstrate that TRAPPII acts as a GEF for Rab11 homologues Ypt31/32 and can also function as a GEF for Rab1, a small GTPase critical for early secretory pathway trafficking (Morozova et al., 2006; Thomas & Fromme, 2016; Yamasaki et al., 2009). The activation of these Rabs by TRAPPII is further regulated by crosstalk with Arf1 GTPase and the Sec7 GEF, ensuring precise temporal and spatial control of vesicle biogenesis at the trans-Golgi network (Thomas & Fromme, 2016). In contrast, TRAPPIII functions as a GEF for Rab1 in both yeast and mammals, where it regulates early secretory pathway trafficking and autophagy (Thomas et al., 2018).

1.5.5 Orthology between yeast and human TRAPP core subunits

Due to the highly conserved nature of the TRAPP complex, structure and composition of each subunit was taken into consideration for assigning the ortholog to each subunit. Significant identity/similarity was found when comparing the amino acid sequence of yeast subunits to human. Orthology was assigned for Bet5 (TRAPPC1), Trs20 (TRAPPC2), Bet3 (TRAPPC3), Trs23 (TRAPPC4), Trs31 (TRAPPC5), and Trs33 (TRAPPC6A/B) (**Table 1.1**) (Sacher et al., 2019).

Yeast Subunit	Human Orthologue	Essential in yeast?	Percent Identity/Similarity (Sacher et al., 2018)
Bet5p	TRAPPC1	Yes	33/54
Trs23p	TRAPPC4	Yes	29/44
Bet3p	TRAPPC3/TRAPPC3L	Yes	56/76
Trs31p	TRAPPC5	Yes	31/52
Trs33p	TRAPPC6A/B	No	35/51, 33/47
Trs20p	TRAPPC2	Yes	34/52
Tca17p	TRAPPC2L	No	24/43

Table 1.1 Yeast and human TRAPP core subunit orthologues, essentiality, and sequence conservation. This table lists the yeast TRAPP core subunits and their human orthologues, indicating whether each subunit is essential for yeast viability. Percent sequence identity and similarity values between yeast and human proteins are taken from Sacher et al., 2018.

1.5.6 Yeast Trapp Core Subunit Organization

In yeast, the TRAPPI complex is composed of seven small core subunits (**Figure 1.2**) which are essential for ER-to-Golgi vesicle tethering (Montpetit & Conibear, 2009). Early foundational studies established TRAPPI as the guanine-nucleotide exchange factor (GEF) for the Rab GTPase Ypt1p (Wang et al., 2000). Genetic interactions showed that mutations in *YPT1* (a gene critical for the early secretory pathway) functionally interacted with *BET3* and *BET5*, two genes encoding core TRAPP subunits (Wang et al., 2000). Biochemical analyses further demonstrated that TRAPPI binds preferentially to the nucleotide-free form of Ypt1p and stimulates GDP–GTP exchange, confirming its GEF activity. Temperature-sensitive alleles of multiple TRAPP subunits failed to catalyze GDP displacement from Ypt1p, supporting the idea that the assembled complex, rather than any single subunit, is required for function. These findings defined TRAPPI as a tethering factor that also catalyzes Rab activation at the cis-Golgi, orchestrating vesicle targeting and fusion (Wang et al., 2000). The structural foundation for these functions was first elucidated by Kim et al., (2006) who resolved the architecture of the yeast TRAPPI

core using a combination of crystallography and electron microscopy. Their study revealed that the seven core subunits form a flat, elongated bi-lobed complex approximately 135 Å in length and 30–75 Å in thickness. This architecture arises through lateral juxtaposition of subunits, with two Bet3p molecules occupying central positions on each lobe, and Bet5p and Trs23p contributing to a symmetrical interface. Trs31p is located at one end of the complex, establishing contacts with Trs23p and Bet3p (Kim et al., 2006). Notably, the crystal structure revealed a large, conserved surface spanning Trs23p, Bet5p, and Bet3p, which forms the functional GEF interface for Ypt1p (Cai et al., 2007). This multivalent binding surface was proposed to hold Ypt1p in a nucleotide-free conformation, enabling GDP release (Cai et al., 2007). The structure also explained the requirement for two copies of Bet3p, each anchoring one side of the complex (Kim et al., 2006), and illustrated how the C-terminal tail of Bet3p inserts into the nucleotide-binding pocket of Ypt1p to facilitate exchange (Cai et al., 2007). Trs31p does not directly bind Ypt1p but is essential for stabilizing the conformation of the exchange surface (Cai et al., 2007). This cooperative, multi-subunit GEF mechanism was a key discovery, distinguishing TRAPP from monomeric GEFs (Cai et al., 2007). Unlike monomeric GEFs, in which a single catalytic domain is sufficient for nucleotide exchange, TRAPP requires the concerted assembly of multiple subunits to generate a composite catalytic surface. Importantly, it demonstrated that activation of Rab GTPases could be coordinated directly at the vesicle tethering site, providing a structural link between membrane tethering and GTPase activation (Cai et al., 2007). These insights provided a framework for understanding not only the TRAPP core but also the modularity of GEF functions across larger TRAPP assemblies.

1.5.7 TRAPP-associated disorders (TRAPPopathies)

“TRAPPopathies” is the collective term for a growing set of rare disorders caused by mutations in genes encoding subunits of the TRAPP complexes (Sacher et al., 2019). TRAPPopathies usually fall into three

major clinical categories: neurodevelopmental disorders, muscular dystrophies, or skeletal dysplasias that often manifest in early life (Hall et al., 2024; Sacher et al., 2019). Moreover, pathogenic variants have been identified in several subunits, and each can give rise to a distinct phenotype. That is because TRAPP complexes are known to regulate fundamental cellular processes such as secretion and autophagy (Lynch-Day et al., 2010; Sacher et al., 2001; Wang et al., 2000). So, a mutation in the complex can lead to devastating effects on patient health, underlying the critical role of TRAPP **Table 1.2, Figure 1.3**

TRAPP Subunit	Primary Disorder	Clinical Presentation	Cellular Phenotype	Other Associated Conditions	Key References
TRAPPC1	TRAPPC1-associated neurodevelopmental syndrome	Profound neurodevelopmental delay, early-onset hypotonia, muscle atrophy	Impaired secretion and autophagy	Expression of antigenic peptides in melanoma (MUM-2 antigen)	(Chiari et al., 1999; Hall et al., 2024; Zykaj et al., 2024)
TRAPPC2	Spondyloepiphyseal Dysplasia Tarda (SEDT)	Short-trunk dwarfism, joint dysplasia, early-onset osteoarthritis	Defective collagen trafficking	None	(Tiller et al., 2001)
TRAPPC2L	Early-onset encephalopathy with episodic rhabdomyolysis	Febrile illness-induced encephalopathy, rhabdomyolysis, spastic tetraplegia	Delayed trafficking, Golgi defects, impaired ciliogenesis	-	(Almousa et al., 2024; Hall et al., 2024)
TRAPPC3	Ciliopathy-like phenotype (tentative)	Postaxial polydactyly, early-onset obesity, developmental delay	Impaired ciliogenesis	-	(Hall et al., 2024)
TRAPPC4	Syndromic neurodevelopmental disorder	Severe developmental delay, seizures, microcephaly	Golgi trafficking defects, autophagy impairment	Colorectal and liver cancer associations	(Van Bergen et al., 2020; Zhao et al., 2011)

TRAPPC5	None reported	-	-	Hepatocellular carcinoma (expression change)	(Hall et al., 2024)
TRAPPC6B	Microcephaly–epilepsy neurodevelopmental disorder	Severe developmental delay, microcephaly, seizures	Likely disrupted trafficking and neuronal signaling	-	(Almousa et al., 2024)
TRAPPC9	Intellectual disability syndrome (MRT13)	Severe ID, microcephaly, autism traits, truncal obesity	NF-κB signaling defects, neuronal outgrowth delay	Cancer (overexpression), inflammatory roles	(Amin et al., 2022; Galindo & Munro, 2023)
TRAPPC10	Neurodevelopmental disorder with microcephaly and short stature	Severe developmental delay, growth retardation	TRAPPII complex destabilization, delayed trafficking	-	(Rawlins et al., 2022)
TRAPPC11	Limb-girdle muscular dystrophy type 2S, multi-system disorder	Muscle weakness, cognitive delay, fatty liver, cataracts	Golgi fragmentation, ER-Golgi delay, protein hypoglycosylation	Congenital Disorder of Glycosylation	(Bogershausen et al., 2013)
TRAPPC12	Progressive early-onset encephalopathy (PEBAS syndrome)	Seizures, brain atrophy, spasticity, hearing loss	Golgi dysfunction, delayed trafficking	-	(Milev et al., 2017)

Table 1.2 Clinical and cellular consequences of mutations in TRAPP subunits. This table summarizes the currently known primary human disorders associated with mutations in TRAPP subunits, along with their key clinical features, cellular phenotypes, and any additional associated conditions. References to primary literature reporting these findings are included. Where available, the table also highlights the broader implications of TRAPP subunit dysfunction.

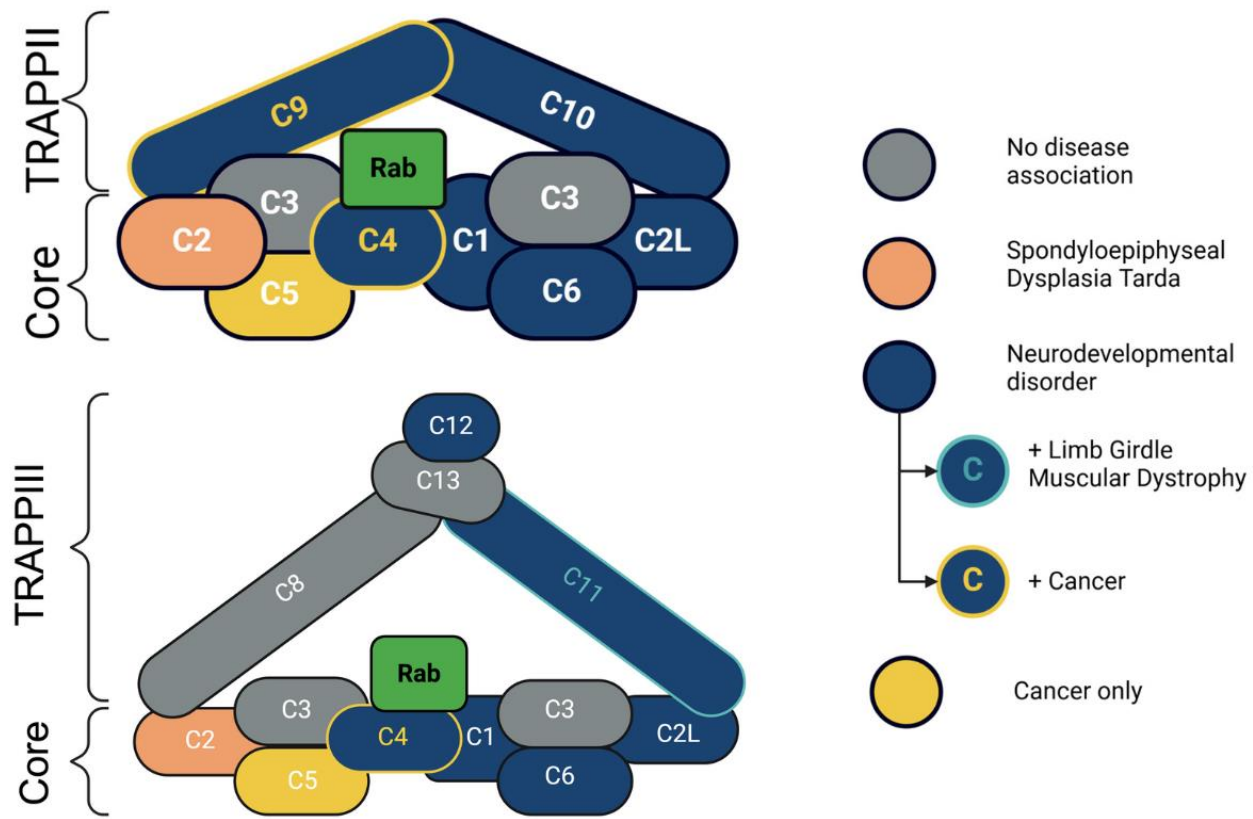


Figure 1.3 Structure summary and associated disorder with each subunit Schematic diagrams of the TRAPPII (top) and TRAPPIII (bottom) complexes, showing the arrangement of core and accessory subunits. Each subunit is colored according to its disease association: grey indicates no known disease association, orange indicates spondyloepiphyseal dysplasia tarda, dark blue indicates neurodevelopmental disorder, and yellow indicates cancer association. Subunits with a turquoise outline and blue circle are associated with both neurodevelopmental disorders and limb girdle muscular dystrophy, while blue subunits with a yellow outline indicate association with both neurodevelopmental disorders and cancer. The “Rab” box indicates the location of Rab GTPase binding. Core subunits shared between complexes are indicated within the bracket (Hall et al., 2024). The bottom panel was modified to accurately represent the geometry of TRAPPIII.

1.6 Previous Work and Objective

1.6.1 Previous work on the humanized model

Previous work on the humanization of the TRAPP complex has shown that TRAPPC1, C2, C2L, and C6A/B could individually substitute for their yeast orthologues (note for simplicity the TRAPP portion of the proteins names will be dropped hereafter) (Zykaj et al., 2024). However, some subunits such as C3, C4, and C5 could not be humanized. This was surprising particularly for C3 which displays high similarity with its yeast counterpart (**Table 1.1**). Work on C1-humanized yeast demonstrated that it is a valid model to characterize VUS (Zykaj et al., 2024).

1.6.2 Objectives

This work provided a strong starting point but also highlighted the need for further investigation into the factors that limit humanization of some TRAPP subunits. We hypothesized that the TRAPP subunits that could not be humanized individually might require the presence of their closest neighboring subunit in the complex for proper incorporation. First, I aim to test whether these subunits can be humanized when co-humanized with their interacting partners. Second, I aim to validate and demonstrate the expression of the genes in the humanized yeast strains. Third, I aim to characterize the resulting strains using growth assays and secretion assays to evaluate their function. Finally, as a proof of concept, I characterize a strain carrying a *TRAPPC3* mutant and compare its phenotype to the wild-type humanized version in yeast through functional assays testing for growth and secretion defects.

2 Materials and Methods:

2.1 Plasmids, Strains, and Media

2.1.1 Plasmids and Yeast strains used in the study:

I show a comprehensive list of all plasmids and yeast strains utilized in this study, including their relevant genetic backgrounds and construction details, is provided in Error! Reference source not found. and **Table 2.2** respectively. These tables serve as a reference for all molecular tools and yeast models employed throughout the experimental procedures described in this work.

Plasmid	Backbone
26	pRS426-Amp <i>TRS33</i> Overproducer
41	pRS426-Amp <i>TRS23</i> Overproducer
579	pDONR201-Kan <i>TRAPPC1</i>
580	pDONR201-Kan <i>TRAPPC3</i>
581	pDONR201-Kan <i>TRAPPC4</i>
582	pDONR201-Kan <i>TRAPPC2L</i>
586	pDONR201-Kan <i>TRAPPC2</i>
607	pGADT70-GWY-AMP <i>TRAPPC6B</i>
612	pDONR201-Kan- <i>TRAPPC5</i>
1258	pRS426-Amp <i>Bet3</i> Overproducer
1805	pCEN6-Cas9-GFP-KanMX
1806	pCEN6-Cas9-GFP-KanMX <i>BET5</i> sgRNA1
1820	pCEN6-Cas9-GFP-KanMX <i>TRS20</i> sgRNA1
1821	pCEN6-Cas9-GFP-KanMX <i>TRS23</i> sgRNA1
1823	pCEN6-Cas9-GFP-KanMX <i>BET3</i> sgRNA1
1824	pCEN6-Cas9-GFP-KanMX <i>TRS31</i> sgRNA1
1826	pCEN6-Cas9-GFP-KanMX <i>TCA17</i> sgRNA1
2046	pCEN6-Cas9-GFP-KanMX <i>C4ΔPDZL</i> sgRNA2

Table 2.1 Plasmids used in this study

<u>Yeast strain</u>	<u>Genotype</u>
90	<i>MATα his4Δ619 ura3Δ52 sec18 mutant</i>
135	<i>MATα his3Δ1 leu2Δ0 lys2Δ0 ura3Δ0</i>
988	<i>MATα his3Δ1 leu2Δ0 lys2Δ0 ura3Δ0 TRS33Δ with C6B</i>
1014	<i>MATα his3Δ1 leu2Δ0 lys2Δ0 ura3Δ0 TCA17Δ TRS33Δ with C2L and C6B</i>
1027	<i>MATα his3Δ1 leu2Δ0 lys2Δ0 ura3Δ0 TCA17Δ TRS33Δ BET5Δ with C1, C2L and C6B</i>
1047	<i>MATα his3Δ1 leu2Δ0 lys2Δ0 ura3Δ0 TCA17Δ TRS33Δ BET5Δ TRS23Δ with C1, C2L, C6B and C4ΔPDZL</i>
1060	<i>MATα his3Δ1 leu2Δ0 lys2Δ0 ura3Δ0 TCA17Δ TRS33Δ BET5Δ TRS23Δ BET3Δ with C1, C2L, C3(L131F), C6B and C4ΔPDZL</i>
1061	<i>MATα his3Δ1 leu2Δ0 lys2Δ0 ura3Δ0 TCA17Δ TRS33Δ BET5Δ TRS23Δ BET3Δ with C1, C2L, C3, C6B and C4ΔPDZL</i>
1098	<i>MATα his3Δ1 leu2Δ0 lys2Δ0 ura3Δ0 Bet3 Overproducer</i>
1099	<i>MATα his3Δ1 leu2Δ0 lys2Δ0 ura3Δ0 Trs33 Overproducer</i>
1100	<i>MATα his3Δ1 leu2Δ0 lys2Δ0 ura3Δ0 Trs23 Overproducer</i>

Table 2.2 Yeast strains used in this study

2.1.2 Media used in this study

The following media were used throughout this study depending on the experimental purpose. Standard YPD medium (1% yeast extract, 2% peptone, 2% glucose) was used for routine yeast growth and propagation. For selection of yeast transformants, YPD supplemented with 200 µg/mL G418 was used to select for kanamycin resistance. Activating medium (YPD with 0.05% glucose and 2% sucrose) was used to induce expression of *SUC2*, the gene encoding invertase. Standard YPD (2% glucose) served as the non-activating control. Synthetic complete dropout media were used for plasmid selection: SC–Ura (synthetic complete medium lacking uracil) and SC–Leu (lacking leucine) were used to maintain plasmids carrying *URA3* or *LEU2* selection markers, respectively.

For bacterial culture, LB medium (1% tryptone, 0.5% yeast extract, 1% NaCl) was used to propagate *E. coli* strains carrying plasmids. Yeast strains were frozen in YPD with 15% glycerol, while bacterial strains were frozen in LB with 15% glycerol and stored at –80 °C for long-term preservation.

2.2 Yeast Transformation and Humanization Protocol

2.2.1 Humanization Using Frozen-EZ Yeast Transformation

Humanization was performed using Frozen-EZ Yeast Transformation II Kit. The appropriate yeast strain was grown overnight in YPD at 30°C with shaking at 200rpm, to reach an OD600 of 0.8-1.0. The cells were harvested and washed with solution I (a wash solution which helps remove excess medium and prepares the cells for future manipulation). The cells were then resuspended with solution II which makes the cells competent for DNA uptake. These competent cells can either be used directly for transformation or can be stored at -80°C for later usage. For the transformation process, 50 ul of competent cells were used, and the appropriate amount of DNA was added (**Table 2.3**). Then, 500 µL of solution III was added to each transformation tube (this solution allows for DNA uptake and increases transformation efficiency). The mixture was incubated at 30°C for 45 minutes with flicking throughout to ensure thorough mixing. The tubes were then centrifuged at 3500 rpm for 4 minutes and resuspended with 750 µL of YPD without shaking to allow for recovery. The recovery step is very important to increase the transformation efficiency before plating on selective media. Once the recovery step is over, 250 µL of cells were plated on YPD + G418 (200 µg/ml) and were incubated at 30°C for 48 hours.

	Empty plasmid	Vector	Repair Template
Competent cells	50µL	50µL	50µL
Solution III	500µL	500µL	500µL
Empty plasmid	500ng	-	-
gRNA	-	500ng	-
gRNA + Repair Template	-	500ng	3.5µg

Table 2.3 Transformation conditions and concentrations. Colonies were inoculated from transformation plates in 3 mL YPD (overnight). 1.5 mL were frozen through resuspension in 750 µL YPD+15% glycerol and then placed in a -80°C freezer. The remaining culture was then used for genomic DNA preparation. All conditions were plated on YPD + G418 (200 µg/ml).

2.2.2 Standard Lithium Acetate Yeast transformation

For non CRISPR-CAS9 transformations the standard lithium acetate/polyethylene glycol (PEG) method was used. Cells were first harvested by centrifugation at 2500 rpm for 2 minutes in a tabletop centrifuge and resuspended in 500 µL of sterile water. The suspension was then transferred to sterile microcentrifuge tubes and centrifuged at maximum speed for 30 seconds. After removing the supernatant, the pellet was resuspended in 250 µL of sterile water. For each transformation, 50 µL of this resuspended cell mixture was transferred into a fresh sterile microcentrifuge tube. The cells were pelleted again by centrifugation at top speed for 30 seconds, and the supernatant was discarded. To each tube, 163 µL of transformation mix was added, followed by 3 µL of plasmid DNA. The transformation mix consisted of 120 µL of 50% PEG 3350 (filter-sterilized), 25 µL of carrier DNA (e.g., denatured salmon sperm DNA), and 18 µL of 1 M lithium acetate (filter-sterilized). The transformation mixture was thoroughly mixed by vortexing and/or pipetting up and down to ensure homogeneity. Following mixing, the tubes were incubated at 42 °C for 45 minutes to allow the DNA to enter the yeast cells. After heat shock, the cells were briefly centrifuged at maximum speed for 30 seconds, and the supernatant was carefully removed. To allow recovery prior to selection, 1 mL of YPD medium was added to each tube, and the cells were incubated at 30 °C for 1 hour with shaking. The transformed cells were then gently resuspended in 300 µL of sterile water, and 150 µL of the suspension was plated onto selective plates to select for successful transformants.

2.2.3 Bacterial Transformation for Plasmid Propagation

Chemically competent *E. coli* cells stored at -80 °C were thawed on ice. Once thawed, 50 µL aliquots of cells were transferred into pre-chilled 15 mL conical tubes, kept on ice. For each ligation reaction, 5–6 µL of plasmid DNA was carefully added directly to the 50 µL droplet of cells at the bottom of the tube, ensuring gentle handling to avoid shearing. The mixture was gently flicked or inverted to mix and then

incubated on ice for 30 minutes to allow the plasmid DNA to bind to the cell surface. Following incubation, the cells were subjected to heat shock at 42 °C for exactly 1 minute to facilitate DNA uptake, then immediately returned to ice to stabilize the cell membranes. Subsequently, 1 mL of LB medium was added to each tube, and the cells were incubated at 37 °C with shaking for 45 minutes to 1 hour to allow expression of antibiotic resistance genes. After recovery, the cells were centrifuged at low speed for 2 minutes to concentrate them prior to plating on selective media.

2.3 Genomic DNA preparation and confirmation

2.3.1 Genomic DNA extraction from yeast cells

Genomic DNA was extracted by first pelleting 1.5 mL of yeast culture at maximum speed for 1 minute, followed by resuspension in 750 µL of sterile water. The cells were then resuspended in 500 µL of spheroplast medium, which consisted of 0.9 M sorbitol, 0.1 M EDTA, 30 mM β-mercaptoethanol, and 0.1–0.5 mg Zymolyase 100T. This mixture was incubated at 37°C in a heat block to allow for cell wall digestion. After incubation, the cells were pelleted again at maximum speed for 1 minute and gently resuspended in 200 µL of Tris-EDTA buffer. To lyse the cells, 30 µL of 10% SDS was added, and the mixture was incubated at 70°C for 15–30 minutes. Protein precipitation was achieved by adding 80 µL of 5 M potassium acetate (KoAc), followed by incubation on ice for 30 minutes to 1 hour. The lysate was centrifuged for 10 minutes, and the supernatant was transferred to a new tube and centrifuged again for another 10 minutes to further clarify the solution. DNA was then precipitated by adding an equal volume of isopropanol to the supernatant and centrifuging for 1 minute. The resulting DNA pellet was washed with 500 µL of 70% ethanol and centrifuged for 30 seconds. Finally, the pellet was air-dried at 37°C for 15 minutes and resuspended in 100 µL of 1X Tris-EDTA buffer.

2.3.2 Confirmation PCR:

The YPD+G418 plates from the transformation contain a mix of humanized and non-humanized colonies. So, an efficient way is needed for screening the colonies. For this reason, the confirmation PCR primers were designed in a way that the forward primer anneals to the 5' yeast untranslated region (UTR) and the reverse primer anneals to the human ORF of interest **Table 2.4**. The PCR reaction was then set up with the subunit specific primers and loaded on 1.5% agarose gel for confirmation **Table 2.5**.

Primer Name	Sequence
TRAPPC1-Fp	GTCCTTACTATTGACTAGTG
TRAPPC1-Rp	CATCCCGTACATCAGCTTATAC
TRAPPC3-Fp	ACTCCAAGCCAAAGGTAAGG
TRAPPC3-Rp	GCCAAGAAATCTTCAATCAGC
TRAPPC2L-Fp	AAGTTCTGCCGGAAGAGCTCATC
TRAPPC2L-Rp	ATTGCGGAGATCTTCTCATCC
TRAPPC6B-Fp	GGAATCTGGTATGCACTCAC
TRAPPC6B-Rp	AACTCATCCTTGAACCTTGCAG
TRAPPC4-Fp	TGTTGGAGTTATGCCTCCTC
TRAPPC4-Rp	GGTCCAAAAGTCCAGCCTT

Table 2.4 Confirmation PCR primers list

Reactants	Volume (μ L)
2mM DNTP	5
5x buffer	10
5 μ M Forward Primer	5
5 μ M Reverse Primer	5
DNA template (Genomic DNA)	1
Polymerase (Q5)	1
dH2O	23

Table 2.5 PCR set up

2.3.3 Sequencing of Humanized Genes

As a final confirmation step, the ORFs are amplified and sequenced using a commercial service. The primers used for PCR sequencing anneal to the regions flanking the 5' and 3' untranslated regions (UTRs), allowing amplification of the entire coding sequence including both UTRs **Table 2.6**.

Sequencing oligos	Sequence
BET5seq-F	CTGGTTGCCTCAGTCGAAATG
BET5seq-R	CCCAAACCAGATCCGAGTTG
TRS20seq-F	CCTCCTCTGCTGAAGTGTAT
TRS20seq-R	GTAACGGAACACTCAAAAGTG
TCA17seq-F	TCACTTCAAGTTCTGCCG
TCA17seq-R	ATATACTACCGGCACCTGATC
TRS33seq-F	CATTAGTAGAACCAAGCGTATCG
TRS33seq-R	GGCTTAAGAAGAGTCCACGA
Bet3seq-F	CGAAACTCCAAGCAAAGGTAAG
Bet3seq-R	ATTGCTTCGCTGGTAAGACAG

Table 2.6 List of primers used for sequencing

2.4 sgRNA Design Cloning

2.4.1 sgRNA Design and Validation

Most of the sgRNA in this project (**Table 2.7**) by using the Geneious software, and the Doench algorithm for high on target low off target activity. with the exception of the *C4* sgRNA which was designed using the IDT website. Testing for the presence of off target effects was done manually using the BLAST website.

sgRNA oligos	Sequence
BET5 sgRNA1-Fp	GACTTTTACACAAAGGCTCTCCAAA
BET5 sgRNA1-Rp	AAACTTGGAGAGCTTTGTGTAAAAA
BET5 sgRNA2-Fp	GACTTGGCTGTTAAAATGACATA
BET5 sgRNA2-Rp	AAACATGTCAATTAAACAGCCAA
TRS20 sgRNA1-Fp	GACTTACCAATGCAGAAATCCACA
TRS20 sgRNA1-Rp	AAACGTGGATTCTGCATTGGTA
TRS20 sgRNA2-Fp	GACTTAGTGATTGCATGCAGTAGAA
TRS20 sgRNA2-Rp	AAACATTCATACGCATGCATCACTA
TCA17 sgRNA1-Fp	GACTTGATTACTGCCCTAATGAGG
TCA17 sgRNA1-Rp	AAACCCCTCATAGGGCAAGTTAACAA
TCA17 sgRNA2-Fp	GACTTTCTGAAGTCAATTTCAT
TCA17 sgRNA2-Rp	AAACATTGAAAAATTGACTTCAGAAA
BET3 sgRNA1-Fp	GACTTCTTCAAGACCTGCATTGCG
BET3 sgRNA1-Rp	AAACCGCAATCGAGGCTTTGAAGAA
BET3 sgRNA2-Fp	GACTTGCTTCAATATGGGCTGCATA
BET3 sgRNA2-Rp	AAACCATAATGCAGCCCATTGAAGC
TRS23 sgRNA1-Fp	GACTTCTTGTAAATAACAAATCAGG

TRS23 sgRNA1-Rp	AAACCCGTATTGTTTATTACAAGAA
TRS23 sgRNA2-Fp	GACTTTATTCTTGCTAGTACACTGCA
TRS23 sgRNA2-Rp	AAACGTGCAGTACTAGCAAGAATAAA
TRS31 sgRNA1-Fp	GACTTGCACCGACCAACAATTCCC
TRS31 sgRNA1-Rp	AAACGGGAATTGTTGGTCAGTGCAA
TRS31 sgRNA2-Fp	GACTTTAGAACCGCTCTTATCAGCAA
TRS31 sgRNA2-Rp	AAACCTGCGATAAAGAGCGCTTCTAA
TRS33 sgRNA1-Fp	GACTTTGCAGCCTGTGGGAAAGATTG
TRS33 sgRNA1-Rp	AAACCAATTCTTCCACAAAGGTGCAG
TRS33 sgRNA2-Fp	GACTTCTCAGCTAGTGGGCATGGAG
TRS33 sgRNA2-Rp	AAACCTCAATGGCCCAGCTAGTAGAGA
C4-pdzl sgRNA1-Fp	TTACCAGTTGGACAGCTACG
C4-pdzl sgRNA1-Rp	CGTAGCTGTCCAAGCTTATGC
C4-pdzl sgRNA2-Fp	TTCTAAATGAGAAGCTTATGC
C4-pdzl sgRNA2-Rp	GCATAAGCTTCTCATTAGAA

Table 2.7 List of sgRNA targeting the genes in yeast

2.4.2 Golden Gate Assembly for sgRNA cloning

The sgRNA was cloned into bacteria using the Golden Gate assembly method. To facilitate cloning with the BsmBI-v2 enzyme, I added specific overhangs to my gRNA oligos. For the forward oligo (5' → 3'), GACTTT was added at the 5' end, followed by the gRNA sequence. For the reverse oligo (also written 5' → 3'), AAAC was added at the 5' end (which anneals to the complementary strand after digestion), followed by the reverse complement of the gRNA sequence, and ended with AA to complete the overhang for ligation.

To prepare the sgRNA inserts for Golden Gate cloning, complementary forward and reverse oligos were annealed prior to ligation. Each oligo was synthesized at a concentration of 100 μM. For annealing, 2 μL of each oligo was mixed with 16 μL of nuclease-free water to reach a final concentration of 10 μM in a total volume of 20 μL. The annealing reaction was performed in a thermal cycler using the following conditions: 95 °C for 15 minutes, decrease temperature by 5 °C every 15 minutes until 25 °C is reached, total reaction duration is approximately 4 hours. The annealed oligos were then diluted 1:1000, and 2 μL of the dilution was used for the Golden Gate assembly.

Golden Gate assembly was used to ligate the annealed sgRNA inserts into a pCEN6-Cas9-GFP-KanX cloning vector (kind gift from Dr. A. Kachroo). The reaction was performed in a 10 µL volume and contained the following components: 20 fmol of circular pCEN6-Cas9-KanMX-GFP vector, which serves as the backbone for cloning; 20 fmol of annealed sgRNA oligos, which provide the insert to be cloned; 1 µL of 10× r3.1 buffer (NEB) to ensure optimal enzymatic activity; 1 µL of BsmBI-v2 restriction enzyme to generate sticky ends by recognizing and cutting outside of its recognition sequence; 1 µL of 10 mM ATP, which provides the energy required for ligation; and 1 µL of T7 DNA ligase to covalently join the compatible overhangs generated by BsmBI digestion. Nuclease-free water was added to reach the final reaction volume.

The reaction mixture was subjected to thermal cycling to enable efficient digestion and ligation. The program consisted of alternating incubations at 37 °C for 5 minutes (to facilitate BsmBI digestion) and 16 °C for 5 minutes (to promote ligation), repeated for 30 cycles. This was followed by a final incubation at 37 °C for 60 minutes and an enzyme inactivation step at 85 °C for 15 minutes. Subsequently, 5 µL of the Golden Gate reaction was transformed into 50 µL of chemically competent *E. coli* cells. Transformants were plated on LB agar supplemented with kanamycin, and green-white screening was used to identify colonies that successfully incorporated the sgRNA insert. In successful transformants, the GFP cassette is excised and replaced by the sgRNA insert at its locus, resulting in white colonies.

2.5 Functional Assays and Expression Analysis

2.5.1 Liquid growth curve yeast assay

Growth curve experiments were conducted using microplate readers at three different temperatures. At 25 °C, absorbance measurements were taken using the Tecan Sunrise microplate reader, while growth at 30 °C and 37 °C was monitored using the LogPhase 600 microplate reader. Yeast cultures were diluted to an initial optical density (OD₆₀₀) of 0.01, and all conditions were tested in at least three biological

replicates. To minimize edge effects and evaporation, the peripheral wells of the 96-well plate were filled with phosphate-buffered saline (PBS). Additionally, a Breath-Easy sealing film (Sigma) was applied to the plate. This film is optically clear, gas-permeable to support aerobic yeast growth, and helps prevent both contamination and evaporation. Growth was continuously monitored over a period of 48 hours.

2.5.2 Spot Dilution Assay

Yeast cultures were adjusted to an OD₆₀₀ of 0.5, and three successive 1:10 serial dilutions were prepared. From each dilution, 2 µL was spotted onto the appropriate solid media. Plates were incubated at the designated temperature (25,30,37°C), and growth was monitored. Images were taken after 24 and 48 hours to assess growth differences across strains and conditions. This experiment was repeated at least three times.

2.5.3 Western blot yeast lysates

The lysates for western blots were prepared in two ways: the spheroplast method and the glass beads method.

For the spheroplast method, 10 OD units of cells were pelleted by centrifugation at maximum speed for 1 minute in a tabletop centrifuge. The pellet was washed with 750 µL of sterile water, then resuspended in 1 mL of spheroplasting buffer (see Genomic DNA Isolation for recipe) and incubated for 1 hour at 37 °C in a heat block. After incubation, cells were pelleted again at maximum speed for 1 minute and washed with 750 µL of spheroplasting buffer without zymolyase. The final pellet was resuspended in 100 µL of Tris-EDTA containing 1% SDS. Protein concentration was determined using the Bradford assay (see Bradford Quantification Assay).

For the glass beads method, 2 OD units of cells were harvested and the supernatant discarded. The pellet was resuspended in 1X SDS-PAGE sample buffer at a volume of 20–30 µL per OD unit. An equal volume

of acid-washed glass beads was added to each tube. The samples were vortexed for 2 minutes, then boiled for 2 minutes. This cycle was repeated a total of three times. Tubes were centrifuged at maximum speed in a microfuge for 1 minute, and the supernatant was transferred to a fresh microcentrifuge tube. Equal volumes of lysate were loaded onto the SDS-PAGE gel.

2.5.4 Invertase Assay

The invertase assay protocol was based on the method described by (Munn et al., 1999). Yeast cells were cultured overnight in YPD medium at permissive temperature until reaching an OD₆₀₀ of 0.2–0.5. For each sample, two OD units of cells were collected and washed with 1 mL of distilled water. Subsequently, two OD units of each yeast strain were resuspended in inducing YP(low D)S (0.05% glucose and 2% sucrose) and non-inducing YPD (2% glucose) media to an OD₆₀₀ of 0.5. The samples were then incubated at restrictive and permissive temperatures for 1 h. Post-incubation, the cells were washed twice with 2 mL of ice-cold 10 mM sodium azide, then adjusted to an OD₆₀₀ of 0.5 using 10 mM sodium azide. Two 0.5 mL aliquots (0.25 OD units each) were transferred to sterile microfuge tubes: one for whole cell invertase activity (external) and one for lysed cell invertase activity (total; external + internal). For whole cells, 50 µL of distilled water was added, and for lysed cells, 50 µL of 10% Triton-X was added. To lyse the cells, two freeze-thaw cycles were performed using liquid nitrogen and room temperature thawing. The assay was prepared on ice. To 20 µL of cells, 25 µL of 0.2 M sodium acetate (pH 4.9) and 12.5 µL of 0.5 M sucrose were added. The sucrose was added to the tube walls to initiate the reactions simultaneously upon centrifugation. The tubes were centrifuged briefly and placed in a 37 °C water bath for 10 min. The reaction was terminated by adding 50 µL of 100 mM potassium phosphate (pH 7), and invertase was inactivated by heating at 90 °C for 3 min. The samples were chilled on ice. Next, 500 µL of assay mix (50 µg/mL glucose oxidase from *Aspergillus niger*, 10 µg/mL horseradish peroxidase, 10 mM potassium phosphate buffer pH 7, 300 µg/mL o-dianisidine, 38% vol/vol glycerol)

was added. The samples were incubated at 30 °C for 20 min. Color development was achieved by adding 750 µL of 6N HCl, and absorbance was measured at A540 using a spectrophotometer.

2.5.5 Gene expression using RT-PCR

Total RNA was extracted from yeast samples using the YeaStar™ RNA Kit (Zymo Research, R1002) following the manufacturer's protocol. Approximately 1–1.5 mL of culture ($1\text{--}5 \times 10^7$ cells) was pelleted and resuspended in YR Digestion Buffer with 5 U of Zymolyase to enzymatically lyse the cell wall. The suspension was incubated at 37°C for 1 hour depending on cell pellet volume. Subsequent lysis was achieved using YR Lysis Buffer, followed by ethanol precipitation and purification through Zymo-Spin™ IIICG columns. To ensure high purity, two wash steps with RNA Wash Buffer were performed before RNA was eluted in 60 µL of DNase/RNase-Free Water.

Real-Time PCR conditions were performed using subunit specific primers **Table 2.9**. For reactions involving the C1 subunit, the reverse primer was used at a concentration of 150 nM instead of the standard 100nM **Table 2.8**.

Reactants	Volume
iTaq Syber mix	5µL
iScript reverse transcriptase	0.125µL
Forward primer 100nM	0.1µL
Reverse primer 100nM	0.1µL
RNA template (up to 500ng)	1µL
Nuclease free water	3.675

Table 2.8 Real-Time PCR components

RT-PCR Primer	Sequence
C1 F	CTCTATCCGCTCGTTGTCAAG
C1 R	CCACGCCAAGTCAGTATTCAATG
C2L F	GGTGGTAGATTCTCCAACACAG
C2L R	CGTCACCATGTTATCAAAGGCC
C4 F	ACGATGAGCGTGTGTTGGTGC
C4 R	CAGATACTCCAGCACCTCTTCC
C6B F	GCCTGCTTACTCAGATGTCTGC
C6B R	CAAGCAGGCATTGAAGACACTTC

Table 2.9 Real-Time PCR primers

2.6 Structural Analysis

2.6.1 Structural Clash Analysis (Pymol)

Structural clash analysis was performed to evaluate the compatibility of humanized and yeast TRAPP core subunits within the multi-protein complex. Atomic models for yeast (PDB: 7e2D) and human subunits were obtained from available PDB structures and AlphaFold predictions, and prepared using PyMOL (Schrödinger, LLC; version 3.0, student license). Each relevant structural model (fully yeast, fully humanized, and partially humanized complexes) was loaded into PyMOL. To assess steric clashes, the show_bumps.py script (available from the PyMOLWiki Script Library) was used. This script calculates van der Waals (vdW) overlaps and displays clashes as red discs (CGO objects). The script was loaded into PyMOL via the command: run ~/Desktop/show_bumps.py For pairwise or complex-wide analysis, relevant selections were created, for example: create pair_bump, (Trappc2 or Trappc3_copy or (7e2d and chain G)) Clash visualization was then performed using: set sculpt_vdw_vis_max, 0.3 show_bumps pair_bump. The cutoff for clash detection was set to 0.3 Å, which highlights only the most significant atomic overlaps and eliminates minor or potentially flexible contacts. Following analysis, clash objects were colored red for visibility.

2.6.2 Structural clash analysis (ChimeraX)

Structural clash analysis was performed to evaluate the compatibility of humanized and yeast TRAPP core subunits within the multi-protein complex. Atomic models for yeast (PDB: 7e2D) and human subunits were obtained from available PDB structures and AlphaFold predictions, and all models were prepared and manipulated in UCSF ChimeraX. Human subunits were substituted for their yeast counterparts using the MatchMaker tool to ensure accurate alignment and positioning. To assess steric compatibility, the ChimeraX Clashes tool was employed with a van der Waals overlap threshold of 0.60

\AA (after a 0.40 \AA reduction for potential hydrogen bonding), flagging atom pairs exceeding this cutoff as clashes. Interactions between atoms separated by four or fewer bonds were excluded, and both intermodel and intramodel clashes were analyzed. Clashes were visualized in real time as red pseudobonds (0.150 \AA radius, four dashes per bond), allowing for continuous monitoring and iterative model refinement. This workflow enabled stringent identification of steric incompatibilities that could arise from humanization or subunit replacement within the TRAPP complex.

3 Results:

3.1 Humanization and validation of the replacement TRAPP core subunits *C1*, *C2L*, and *C6B*

Previous work from our laboratory (Zykaj et al., 2024) established that humanized yeast serves as an efficient system to study TRAPP variants of unknown significance (VUS) in the absence of human cell lines. The CRISPR-based humanization strategy involved introducing a plasmid encoding Cas9 and an sgRNA targeting the yeast orthologue. This system induces a double-stranded break (DSB) in the yeast genome, which is repaired using a human ORF as the repair template. The plasmid also confers G418 resistance for selection on YPD+G418 plates. After PCR validation and sequencing confirmation of correct integration, strains were streaked on YPD to eliminate the plasmid and G418 resistance, ensuring scarless replacement of the yeast gene with its human counterpart while maintaining an otherwise fully yeast background.

Previous work showed that subunits *C1*, *C2*, *C2L*, and *C6B* could each be individually humanized, whereas *C3*, *C4*, and *C5* could not (Zykaj et al., 2024). We hypothesized that the inability to humanize some subunits might be due to their requirement for humanized neighboring subunits within the complex. Therefore, I began constructing a stepwise humanized TRAPP core complex, starting with a strain containing *C6B*, followed by sequential addition of *C2L* and *C1* (**Figure 3.1**). Although each of these subunits is humanizable on its own, this approach allowed us to build a partially humanized TRAPP core in a yeast background.

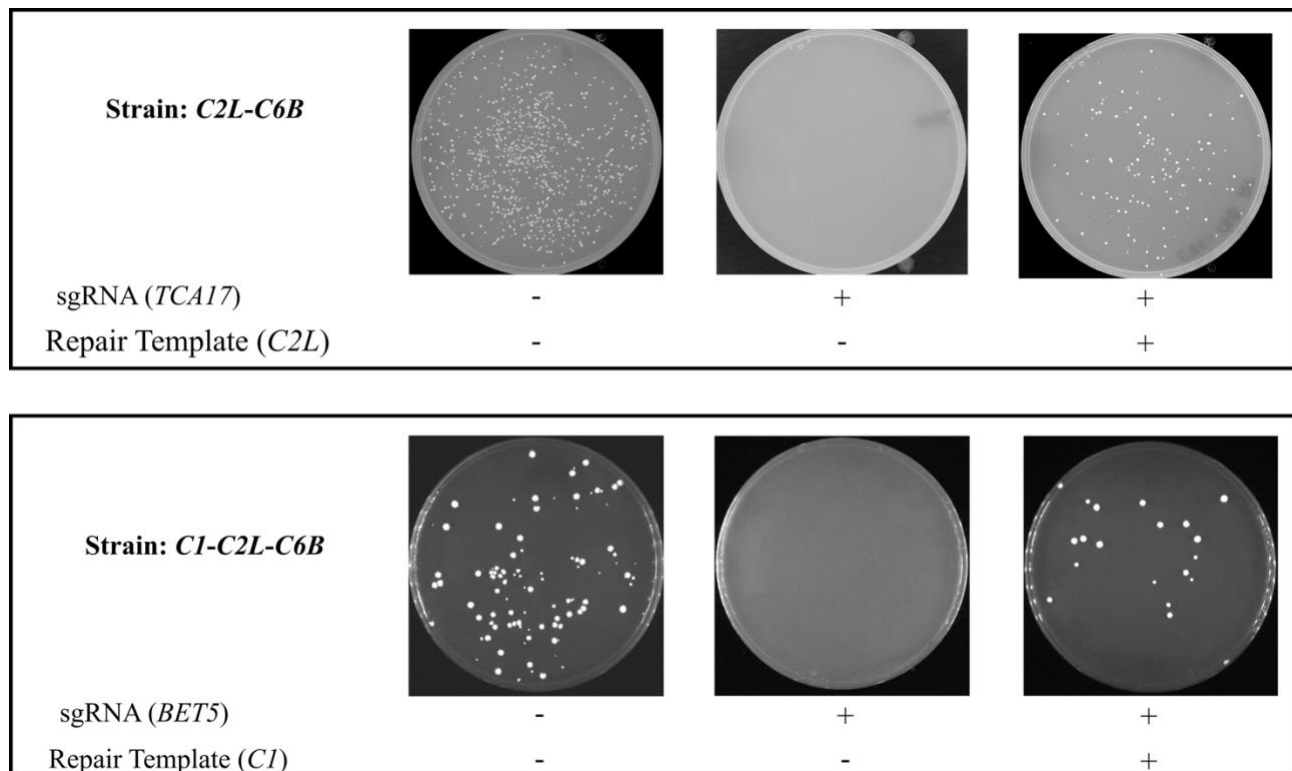


Figure 3.1 CRISPR-Cas9-mediated humanization of TRAPP complex subunits in yeast. The column with no sgRNA and no repair template (empty plasmid) serves as a control for demonstrating baseline transformation efficiency. sgRNA without repair template is a control to verify the specificity of the sgRNA; absence of growth confirms that sgRNA double stranded breaks are lethal without repair. sgRNA with repair template shows successful integration of the human TRAPP subunit ORF as indicated by colony growth. All plates were grown on YPD+G418 selective media to confirm successful humanization.

To confirm successful humanization, PCR followed by Sanger sequencing verified the scarless integration of these three human subunits (**Figure 3.3**). Confirmation PCR using subunit-specific primers further demonstrated correct integration, with products resolved by size on an agarose gel (**Figure 3.2**).

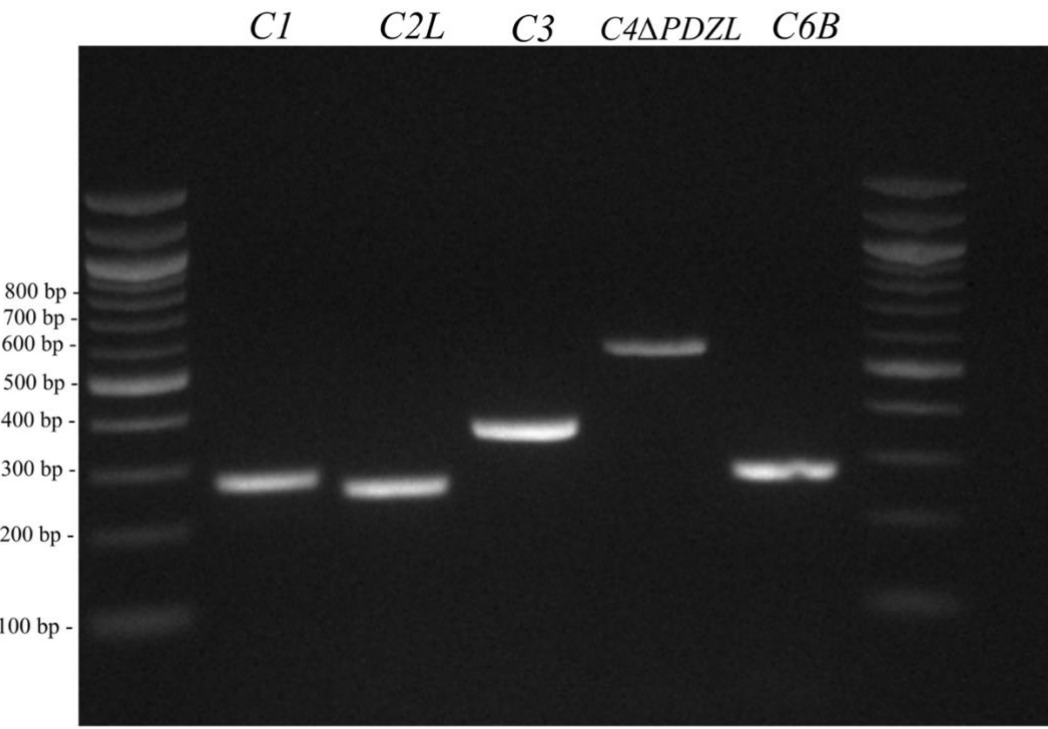


Figure 3.2 Confirmation PCR of all human subunits Confirmation PCR shows the successful replacement of the humanized subunit, PCR was performed using specific confirmation primers for each subunit. The expected band size for each successful transformation is 274 bp for *C1*, 255 bp for *C2L*, 361 bp for *C3*, 562 *C4ΔPDZL*, 276 bp for *C6B*.

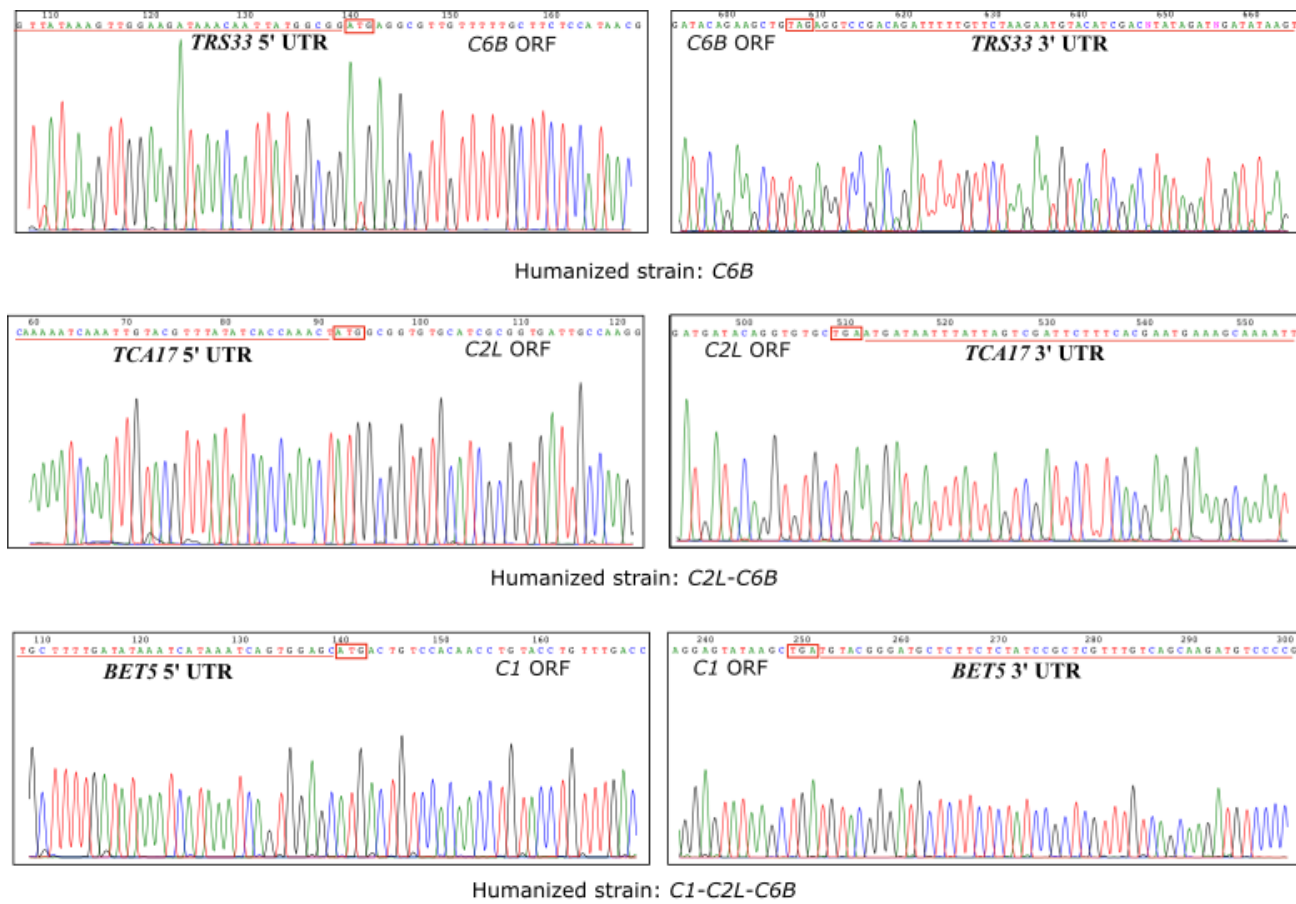
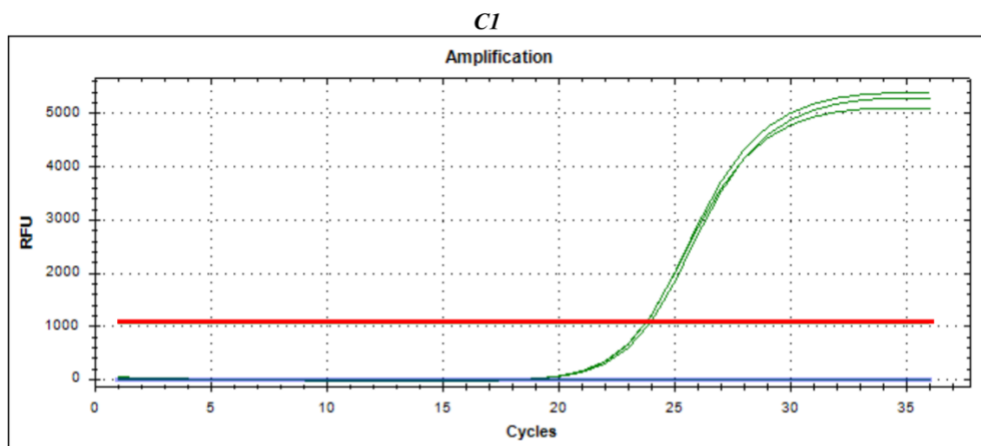


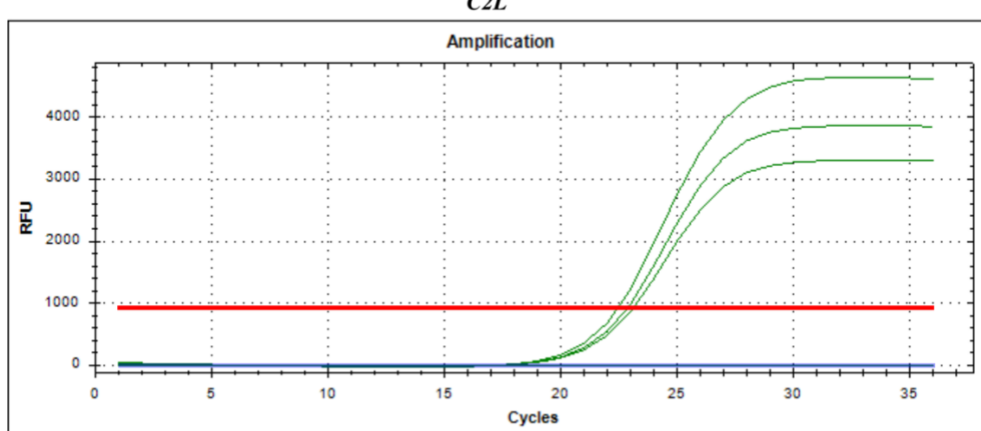
Figure 3.3 Sanger Sequencing of *C1*, *C2L*, and *C6B*. Genomic DNA from each humanized yeast strain was PCR-amplified and subjected to Sanger sequencing. The red boxes indicate the start and stop codons of the integrated human open reading frames (ORFs), while the underlined regions correspond to the upstream and downstream untranslated regions (UTRs) of the endogenous yeast genes. These chromatograms confirm scarless replacement of the yeast ORFs with their human counterparts, validating precise genomic integration for each construct.

Due to the lack of suitable antibodies for many of the human TRAPP proteins, we used real-time PCR to confirm the expression of human *C1*, *C2L* and *C6B* transcripts in the humanized strains. Ct values of 23.82 ± 0.07 , 22.14 ± 0.16 , 22.02 ± 0.07 were detected for *C1*, *C2L* and *C6B*, respectively, in the humanized strain, while the parental strain showed no detectable expression (Figure 3.4), confirming expression of the human genes.

A.



B.



C.

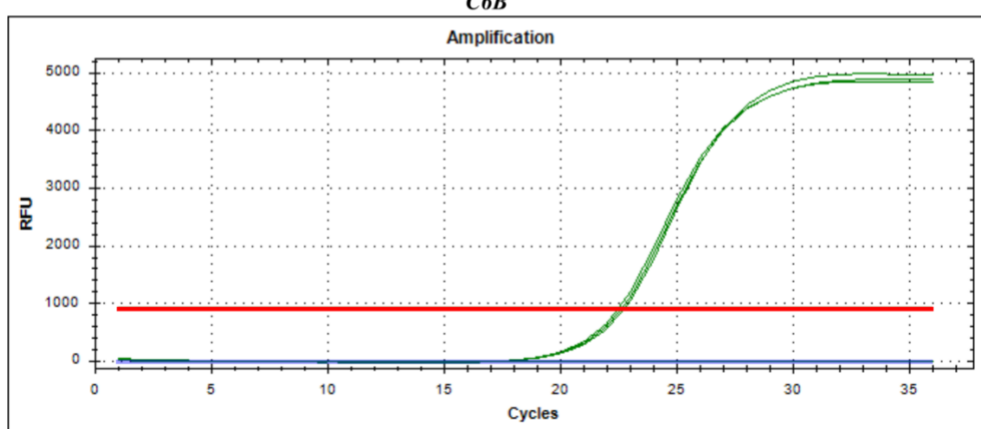


Figure 3.4 Real Time PCR showing expression of C2L, C4 Δ PDZL, and C6B. (A) RT-PCR amplification curves for *C1*, (B) *C2L*, (C) *C6B*, each showing three biological replicates as distinct peaks. In all panels, the blue flat line at the baseline represents the parental yeast strain, demonstrating no amplification because the RT-PCR primers are specific to the human subunit sequences. An

amplification threshold of 1000 RFU (relative fluorescence units) was applied, and only samples expressing the humanized genes exceeded this value. These results confirm specific and robust expression of human *C2L* and *C6B* in the humanized yeast strains.

To further confirm replacement of Trs33 with C6B, Western analysis was performed using an antibody against the yeast protein Trs33. As expected, the parental strain and Trs33 overproducer displayed a Trs33 band, whereas the humanized strain did not, consistent with replacement of the yeast Trs33 (**Figure 3.8 D**). Collectively, these results confirm successful humanization, correct integration, and expression of the human TRAPP core subunits C6B, C2L and C1 in yeast.

3.2 Humanization of C4 and C3 subunits and unsuccessful restoration of the PDZL domain

To further humanize the TRAPP complex, I decided to add more subunits in the strain that contains C1, C2L, C6B. I next targeted the C4 subunit, which interacts directly with C1 (Menon et al., 2006). Initial attempts to replace yeast TRS23 with full length human C4 were unsuccessful

Figure 3.5. Drawing inspiration from previous work showing that making human proteins more yeast like can enhance compatibility (Sultana et al., 2023), we examined the structural differences between C4 and Trs23p. We previously found that human C4 contains a PDZL domain that is absent in yeast (Sacher et al., 2008), so a truncated version lacking this domain (C4 Δ PDZL) was generated which made it more similar to the yeast protein. This construct was able to successfully replace the yeast gene

Figure 3.5. However, when further modified by adding the SMS domain from yeast Trs23p, the replacement was unsuccessful. These results demonstrate that targeted domain removal can enable humanization of C4, but that additional modifications do not always improve compatibility and may actually hinder successful functional integration.

After establishing that C4 Δ PDZL could be successfully humanized I next attempted to humanize C3 in this partially humanized background. Importantly, previous attempts to humanize C3 in isolation were

unsuccessful; however, when *C3* was introduced into the background already containing humanized *C4ΔPDZL-C1-C2-C6B*, successful replacement was achieved (**Figure 3.6**). This finding demonstrates that prior humanization of certain neighboring subunits, particularly *C4ΔPDZL*, is required to enable subsequent humanization of *C3*, highlighting the importance of context and compatible protein-protein interactions within the assembly of the TRAPP complex. The resulting strain, containing *C2L*, *C6B*, *C1*, *C4ΔPDZL*, *C3*, *TRS31*, and *TRS20*, is hereafter referred to as the Partially Humanized TRAPP Core (PHTC).

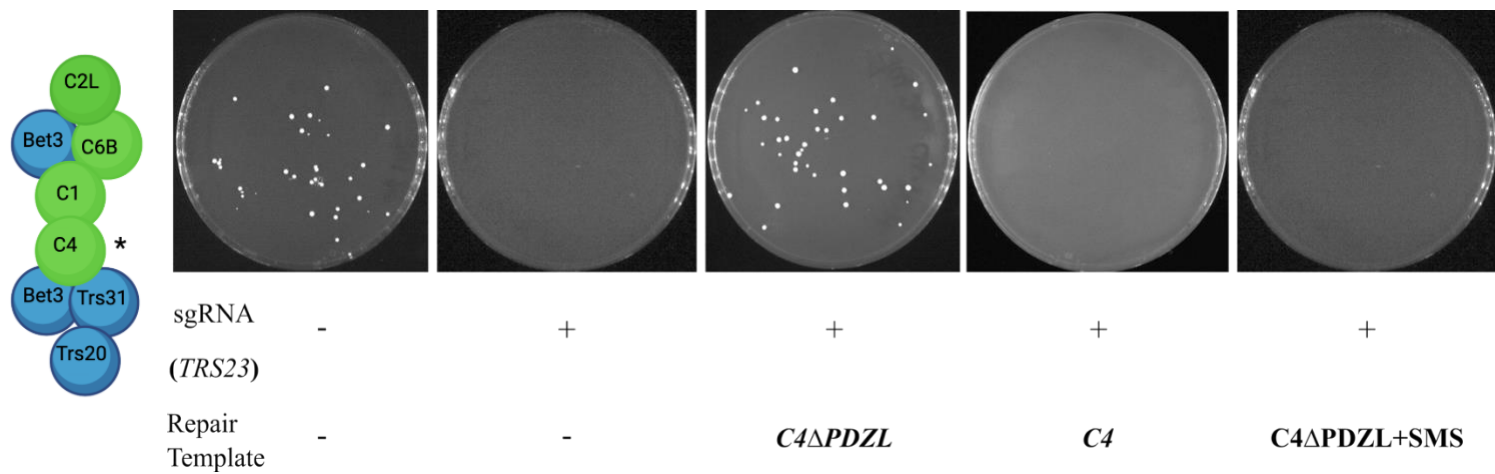


Figure 3.5 Successful humanization of *C4ΔPDZL*. Yeast transformation plates showing the outcome of attempts to repair the *Trs23* double-strand break (DSB) with various repair templates: *C4ΔPDZL*, *C4*, and *C4ΔPDZL+SMS*. Plates contain YPD with G418 for selection. The presence of colonies indicates successful CRISPR-mediated replacement of the yeast gene with the humanized construct in the presence of both sgRNA (targeting *TRS23*) and the appropriate repair template. See **Figure 3.1** legend for explanation of controls.

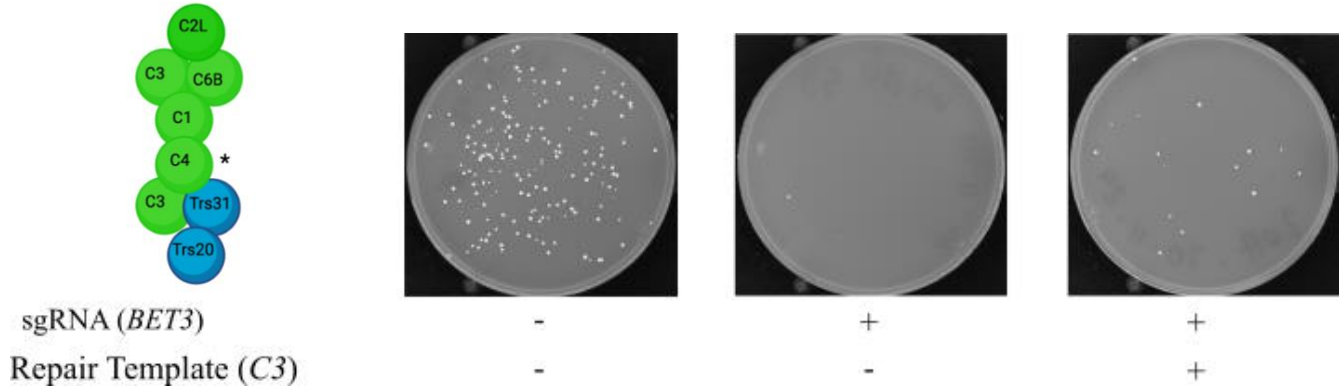


Figure 3.6 Successful humanization of *C3* Yeast transformation plates showing the CRISPR-Cas9 mediated replacement of *TRS31* with human *C3*. Colonies on YPD+G418 selection plates are observed only when both the sgRNA (targeting *TRS31*) and the *C3* repair template are present, indicating successful integration of the human *C3* sequence. See **Figure 3.1** legend for explanation of controls.

To confirm successful replacement, confirmation PCR was performed for both *C3* and *C4ΔPDZL*, and the results demonstrated integration of the human genes at the expected loci (**Figure 3.2**). Scarless gene replacement was further validated by Sanger sequencing, confirming the precise substitution of the yeast genes with their human counterparts (**Figure 3.7**). The expression was then assessed by western blot for both humanized subunits and RT PCR for *C4ΔPDZL*. Western blot analysis using an antibody against human *C3* (**Figure 3.8 A**) showed a band in the humanized strain, while no band was detected in the parental strain or in the strain overexpressing yeast Bet3, confirming the specific expression of human *C3*. When the membrane was probed with an anti-Bet3 antibody (**Figure 3.8 B**), a band was present in the parental and Bet3 overproducer strains, but absent in the humanized strain, consistent with replacement of Bet3 by the human protein. For *C4ΔPDZL*, a similar approach was used: western blotting with an anti-Trs23 antibody (**Figure 3.8 C**) detected a band in the parental and Trs23 overproducer strains, but not in the strain where Trs23 was replaced. The presence of human *C4ΔPDZL* transcript was further confirmed by RT PCR ($C_T: 20.34 \pm 0.03$) providing additional evidence for successful expression (**Figure 3.9**).

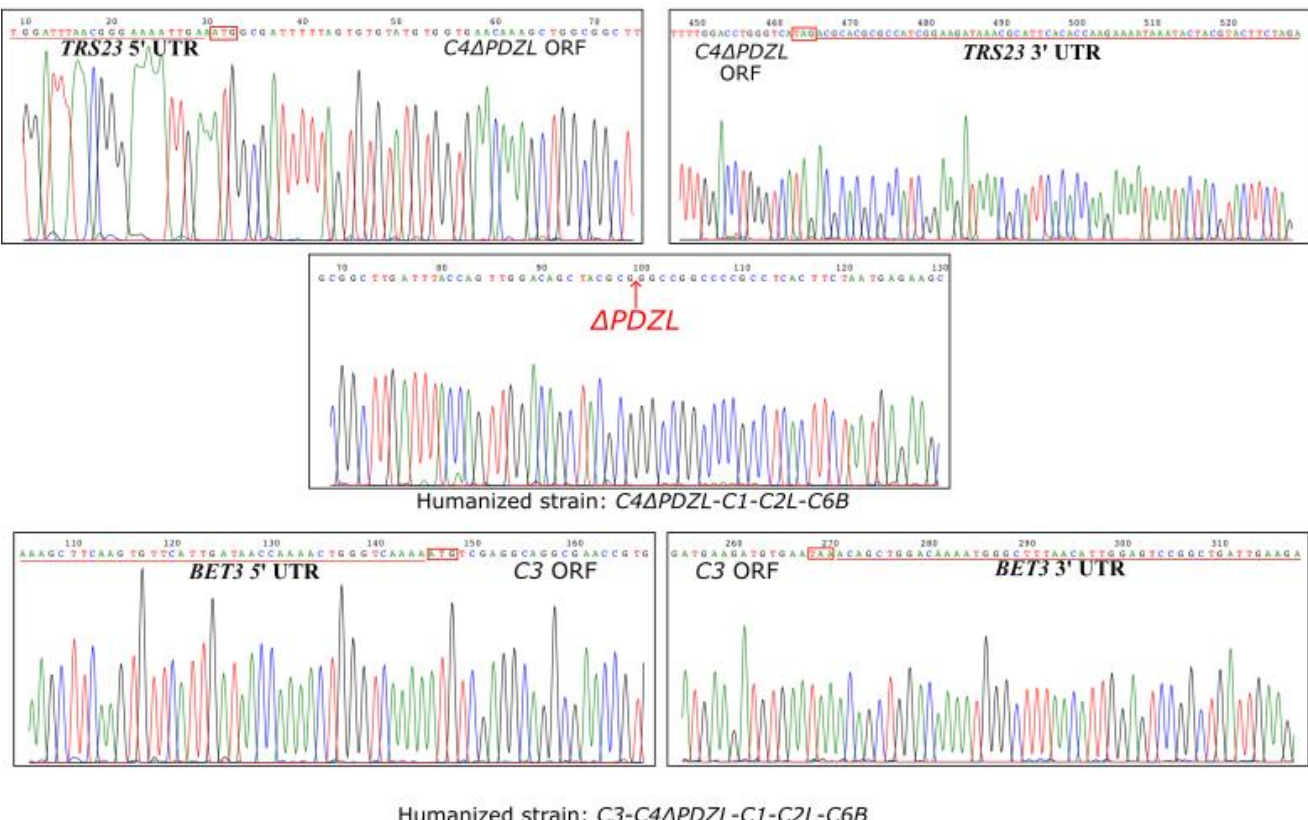


Figure 3.7 Verification of successful C4 Δ PDZL and C3 scarless replacement via Sanger sequencing. Chromatograms from Sanger sequencing confirm the seamless integration of human C4 Δ PDZL and C3 ORFs into the yeast genome. The sequences show the expected junctions between yeast 5' and 3' untranslated regions (UTRs) and the inserted human ORFs, demonstrating scarless replacement. For C4 Δ PDZL, the characteristic Δ PDZL region is indicated. These results verify precise genome editing and successful humanization of the indicated strains.

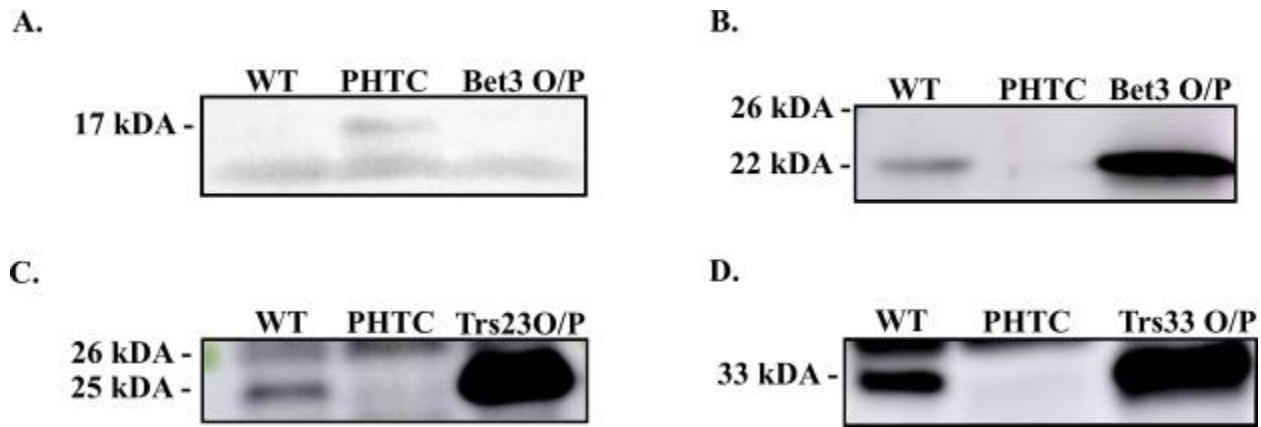


Figure 3.8 Western blots showing expression of the humanized C3 and C4 Δ PDZL subunits. Panel A: Western blot probed with anti-C3 antibody shows the presence of the human C3 band in the partially humanized TRAPP core complex (PHTC), but not in the parental strain or the Bet3 overexpression control, indicating successful humanization and expression of C3. Panel B: Blot probed with anti-Bet3 antibody for the same samples. The absence of a Bet3 band in the PHTC lane, where human C3 replaces yeast Bet3 (as shown in A), further confirms C3 expression. Panel C: Blot probed with anti-Trs23 antibody for parental, PHTCC, and Trs23 overexpression strains. The lack of a Trs23 band in the PHTC lane indicates that the yeast Trs23 has been successfully replaced, verifying efficient humanization at this position. Panel D: Western blot was probed with anti-Trs33 antibody. Lanes correspond to the parental strain, PHTC, and a Trs33 overexpression strain. The absence of a band in the PHTC lane demonstrates the lack of expression of Trs33.

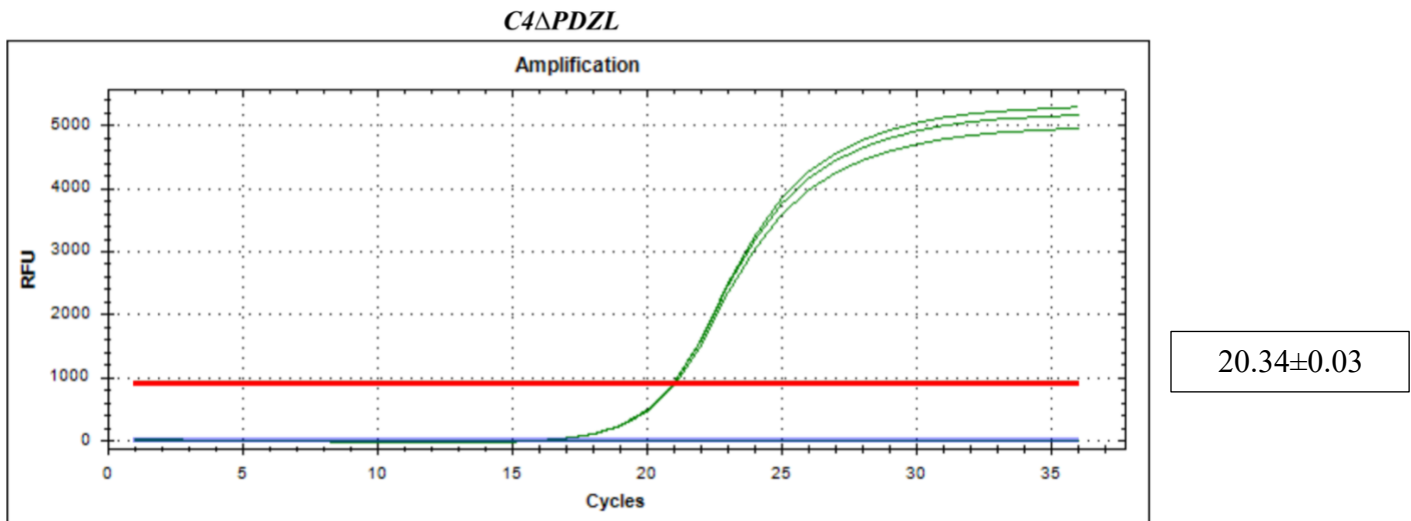


Figure 3.9 Real Time PCR for *C4ΔPDZL* in PHTC. (A) RT-PCR amplification curves for *C4ΔPDZL*, showing three biological replicates as distinct peaks. In all panels, the blue flat line at the baseline represents the parental yeast strain, demonstrating no amplification because the RT-PCR primers are specific to the human subunit sequences. The red line is the threshold for amplification was set at 1000 RFU (relative fluorescence units), and only samples expressing the *C4ΔPDZL* humanized genes crossed this threshold.

Together, these findings demonstrate that both *C3* and *C4ΔPDZL* can functionally replace their essential yeast orthologues. This result underscores the importance of context-dependent humanization, where maintaining compatibility between protein–protein interactions within the complex is critical for successful assembly and function. Achieving functional expression of these essential subunits in yeast not only advances the construction of a fully humanized TRAPP core, but also establishes a valuable platform for studying human variants in a tractable eukaryotic model.

After successfully humanizing *C3* in the context of the PHTC strain, I next attempted to restore the *PDZL* domain in *C4*, hypothesizing that the presence of humanized *C3* might enable successful replacement with the full length human *C4*. Because *C4ΔPDZL* was already present in the PHTC strain, a new sgRNA

was designed to specifically target the *C4ΔPDZL* allele (**Table 2.7**). The full length *C4* open reading frame was provided as a repair template for homologous recombination. However, this attempt to restore the *PDZL* domain was unsuccessful, as indicated by the absence of colonies on plates containing both the new sgRNA and the repair template (**Figure 3.10**). To investigate the structural basis for the lack of viability, I performed clash analysis using ChimeraX which will show any van der Waals overlap (**Figure 3.11**). In PHTC context, a clash appears between *C1* and *C4ΔPDZL*, however this clash is not lethal as *C4ΔPDZL* can still replace *Trs23* in yeast (**Figure 3.11 A**). However, whenever *C4* is replaced in PHTC new and more pronounced clashes with *C3* appear (**Figure 3.11 B**). These results suggest that even in the presence of humanized *C3*, the addition of the *PDZL* domain is not tolerated in yeast, further highlighting the challenge of integrating human specific domains into the TRAPP core complex.

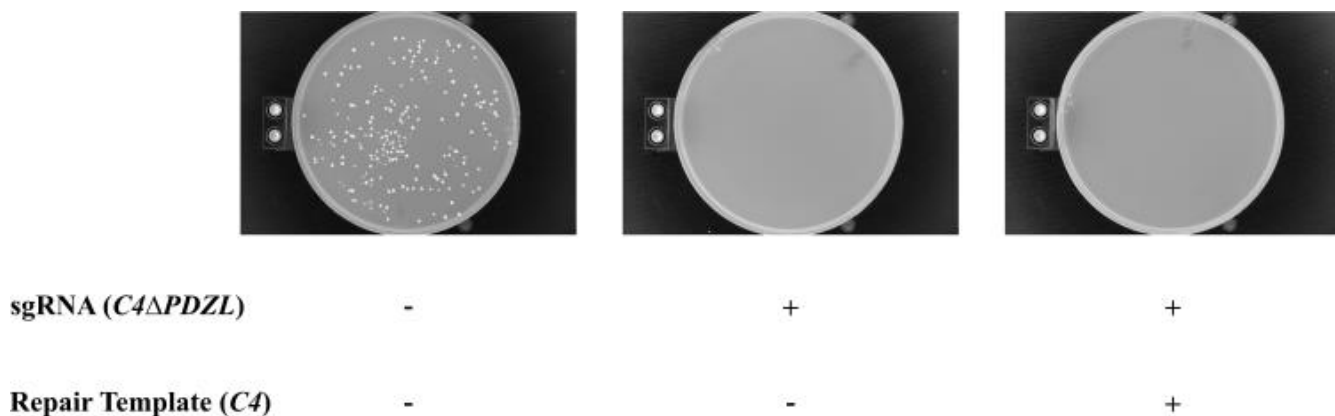
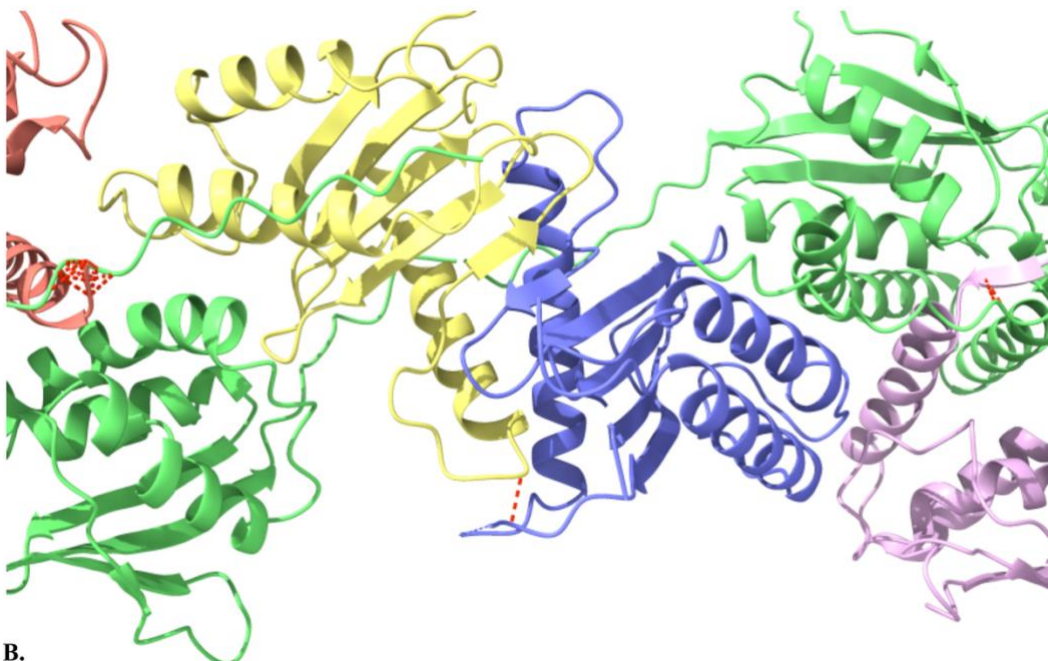


Figure 3.10 Attempted replacement of human C4ΔPDZL with full-length C4 ORF. CRISPR-Cas9 editing was performed in a strain expressing PHTC. A sgRNA was designed to target the integrated human *C4ΔPDZL* sequence, and the repair template used encoded the full-length human *C4* open reading frame (ORF). No colonies are observed in the plate that contains the sgRNA with the repair template, indicate unsuccessful replacement. See **Figure 3.1** legend for explanation of controls.

A.



B.

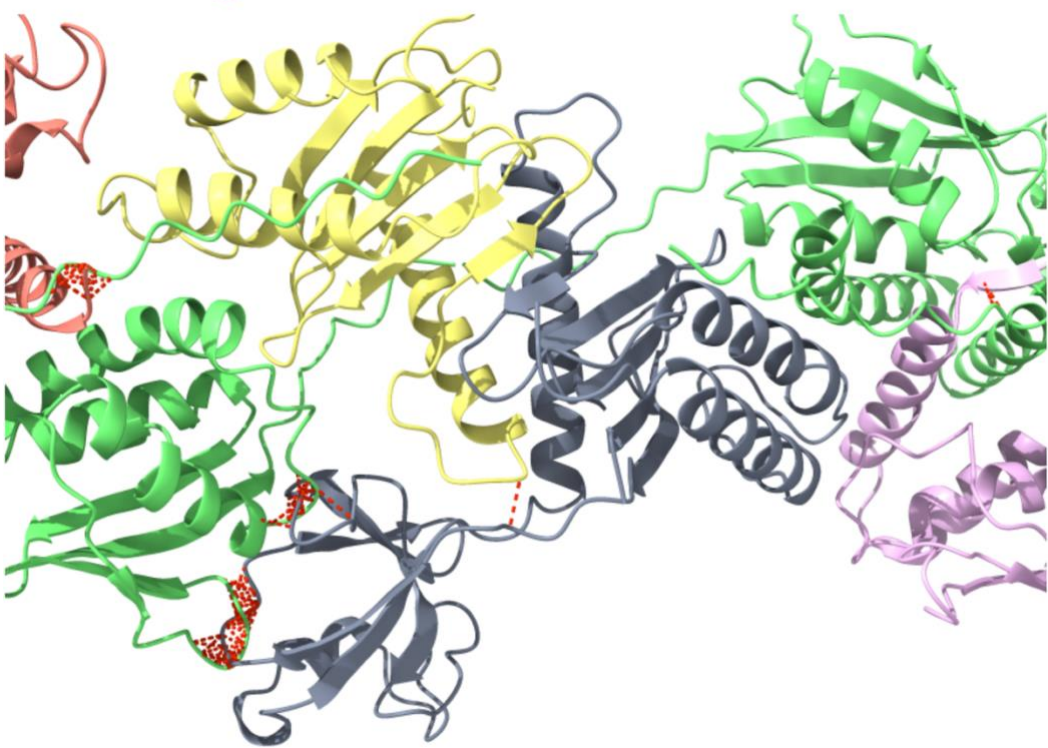


Figure 3.11 Clashes of C4 Δ PDZL vs C4 in PHTC (A) Structure showing the C3 (green), C1 (yellow), and C4 Δ PDZL (purple) subunits. Dashed red lines indicate steric clashes detected using ChimeraX's built-in clash analysis tool with the following parameters: VDW overlap $\geq 0.60 \text{ \AA}$ (after subtracting 0.40 \AA for H-bonding), center-to-center distance $\leq 4.0 \text{ \AA}$, with at least one end selected. Interactions between

atoms \leq 4 bonds apart were ignored, but no interactions were excluded based on sequence separation (i.e., residues \leq 5 apart in sequence were included). Only intermodel and intramolecular interactions were included. Pseudobonds representing clashes are displayed in red. (B) Same as (A), except the C4 subunit with intact PDZL domain is shown in nickel color.

3.3 *C2* and *C5* could not replace their orthologues *TRS20* and *TRS31* in the PHTC strain

Given that we constructed a strain (PHTC) that contains all human TRAPP core subunits except for *C5* and *C2*, we next attempted to complete the core by adding the ORFs encoding these subunits. Attempts to replace yeast *TRS31* with human *C5* were unsuccessful, as evidenced by the lack of viable colonies following transformation on G418 plates(**Figure 3.12**). Additionally, efforts to humanize *C2* in the PHTC background did not result in successful replacement of *TRS20*. This result was unexpected, as human *C2* was previously shown to successfully complement *TRS20* in the parental yeast strain but failed to do so in the context of the PHTC background (Zykaj et al., 2024). These findings suggest that the ability of certain human subunits to functionally replace their yeast counterparts may be highly dependent on the broader context of the complex and the specific combination of humanized subunits present.

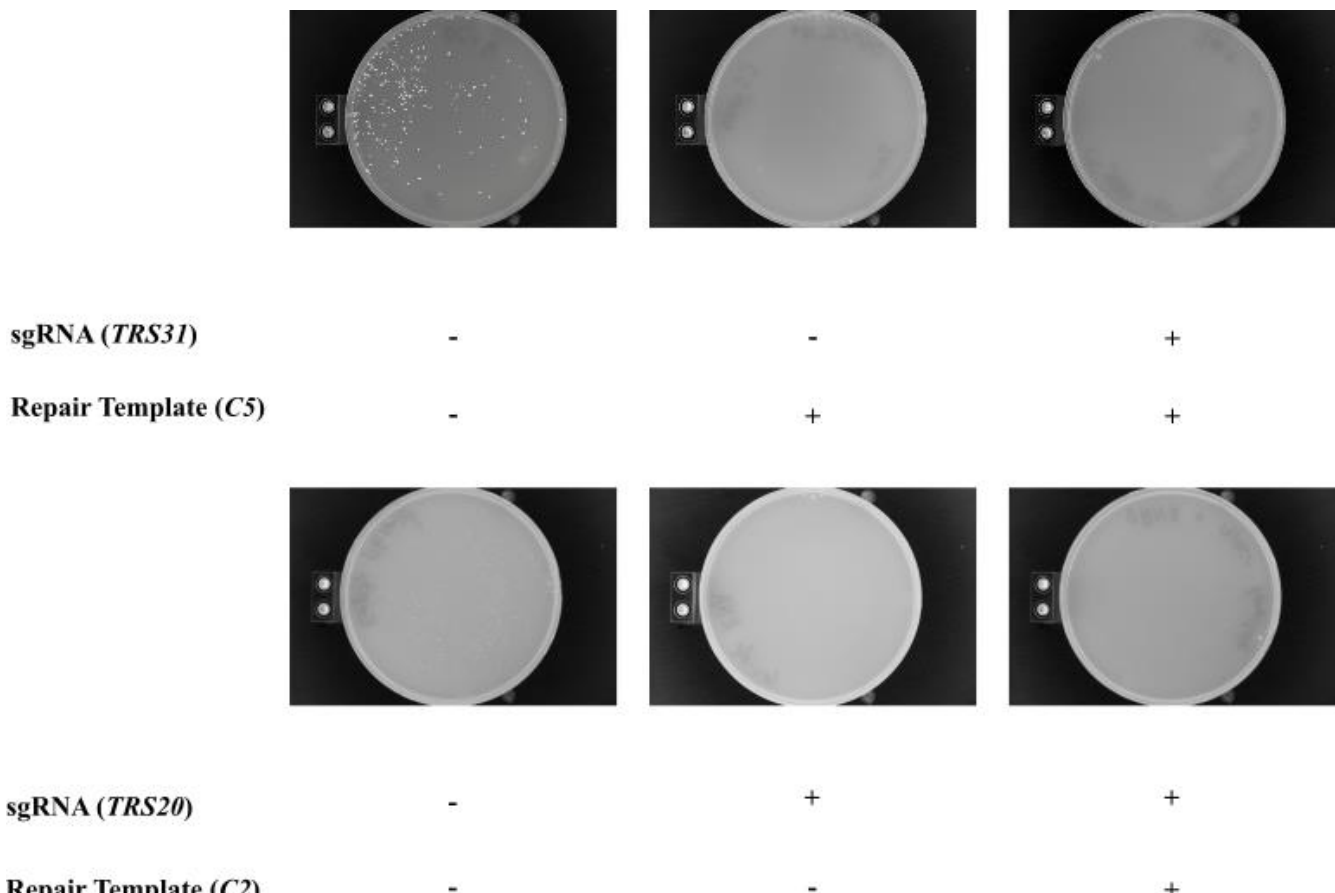


Figure 3.12 CRISPR-Cas9-mediated humanization of *C5* and *C2* in a PHTCC background. All transformations were performed in the PHTCC strain. The top panel shows targeting of the *TRS3I* gene using a sgRNA and a repair template encoding *C5*. The bottom panel shows targeting of the *TRS20* gene using a sgRNA and a repair template encoding *C2*. No colonies are observed in the plate that contains the sgRNA with the repair template, indicate unsuccessful replacement. See *Figure 3.1* legend for explanation of controls.

3.4 Structural modeling and clash analysis of PHTCC

To assess how sequential humanization affects structural compatibility among TRAPP subunits, stepwise structural modeling of the humanized strain was performed, reflecting the order of experimental subunit replacement. In the parental strain, no steric clashes were observed (not shown). Replacement of Trs33

with C6B introduced clashes between C6B and Bet5 (**Figure 3.13 A**). Substitution of Tca17 with C2L did not result in additional clashes (**Figure 3.13 B**). Subsequent replacement of Bet5 with C1 led to new clashes between C1 and Trs23 (**Figure 3.13 C**). Introduction of C4ΔPDZL in place of Trs23 generated further clashes, specifically between C4ΔPDZL and C1, as well as C4ΔPDZL and Bet3 (**Figure 3.13 D**). Finally, replacing Bet3 with C3 resulted in clashes between C3 and C6B and between C3 and Trs31 (**Figure 3.13 E**). Notably, the clashes previously observed between Bet3 and C4ΔPDZL were no longer present after the replacement with C3. These results demonstrate that progressive humanization of the TRAPP complex can lead to the emergence or resolution of structural incompatibilities, suggesting that the stability of the humanized complex is context-dependent and influenced by the specific combination of subunits present.

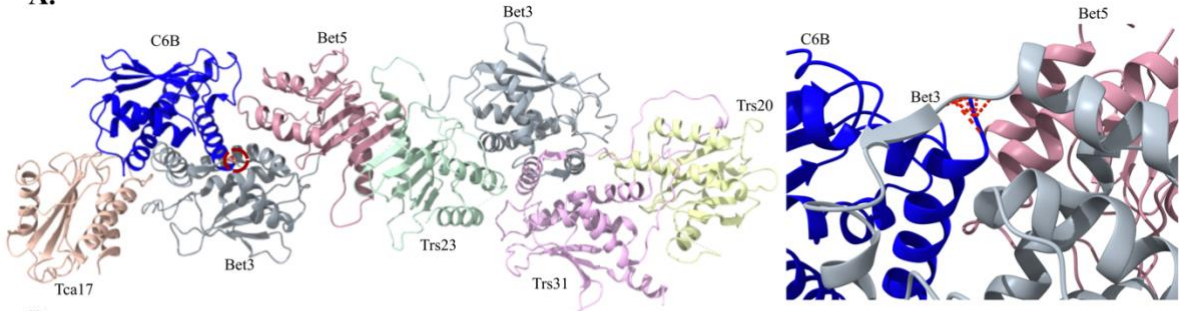
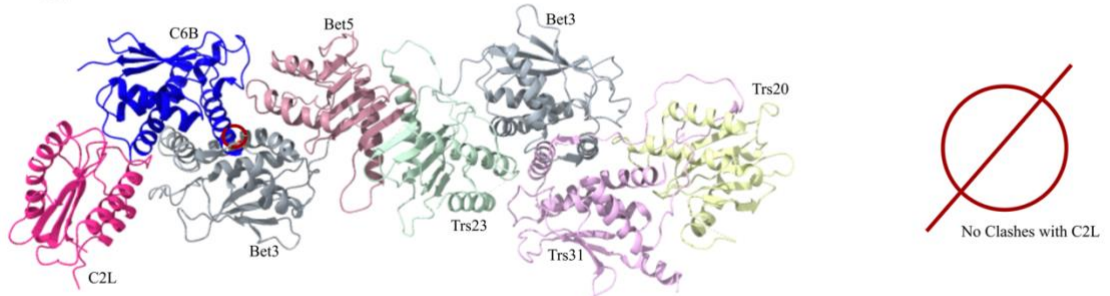
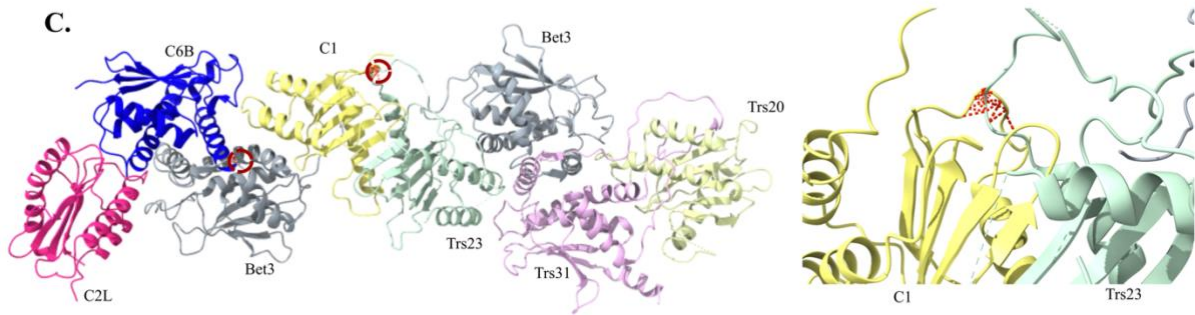
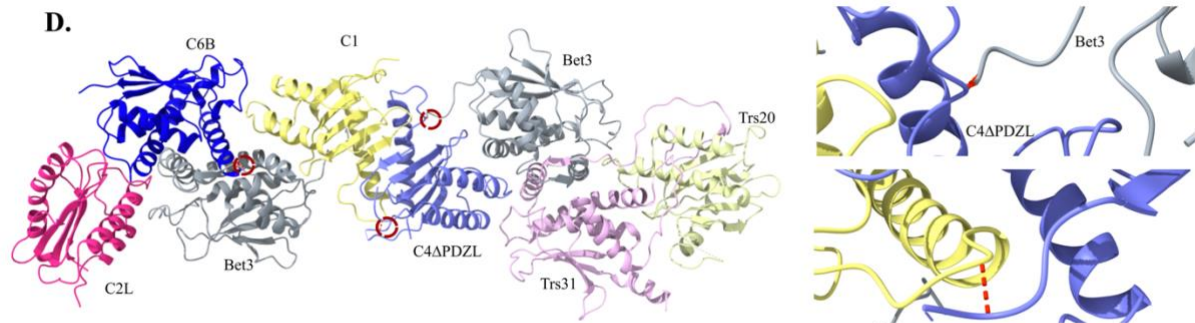
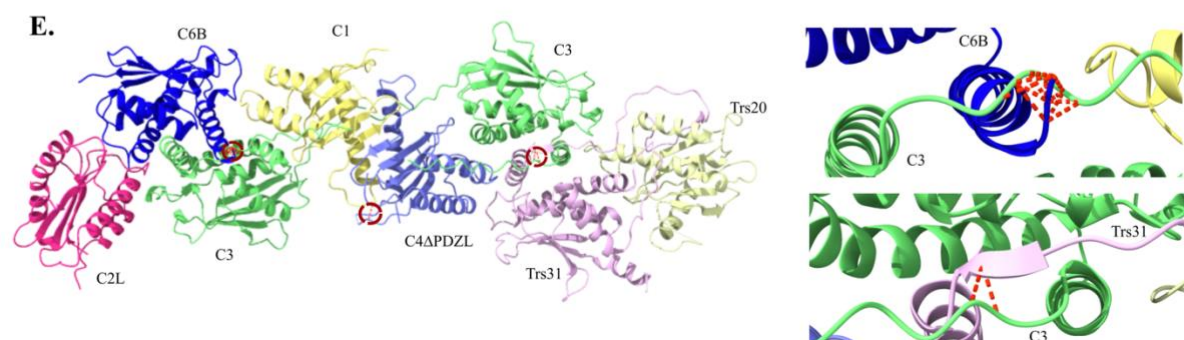
A.**B.****C.****D.****E.**

Figure 3.13 Sequential humanization of the TRAPP core reveals emergence of subunit-specific steric clashes by structural modeling. For each step, the left panel shows the overall structure of the TRAPP core complex with the indicated subunit replaced by its human ortholog, and the right panel shows a zoomed-in view of the corresponding steric clash. Clash analysis was performed in ChimeraX using the parameters shown (bottom), with only new clashes emerging after the addition of each human subunit displayed. Red circles in the overview panels indicate the position of the clash; zoomed-in views highlight the detailed atomic overlap (red dashed lines). Only clashes appearing after humanization at each stage are shown. Panel descriptions: A: C6B replaces Trs33 B: C2L replaces Tca17 C: C1 replaces Bet5 D: C4 Δ PDZL replaces Trs23 E: C3 replaces Bet3 Clash detection parameters: VDW overlap $\geq 0.60 \text{ \AA}$ after subtracting 0.40 \AA for H-bonding, ignoring interactions between atoms 4 or fewer bonds apart, and excluding interactions between residues <5 apart in sequence. Both intermodel and intramodel clashes are included. Clashes are displayed as red dashed pseudobonds (radius 0.15, 4 dashes).

3.5 Sequential humanization of *C2*

To better understand the conditions under which *C2* can replace *TRS20*, I performed a sequential humanization approach by introducing *C2* into various combinations of humanized strains (**Figure 3.14**). The results showed that *C2* could successfully replace *TRS20* only in the parental strain and in a strain where *C2L* was also humanized. In all other humanized combinations tested, *C2* replacement was unsuccessful. This demonstrates that the ability of *C2* to complement its yeast orthologue is highly context dependent: it functions in the presence of humanized *C2L* but fails when additional subunits are humanized. These findings highlight the complexity of multisubunit assembly and suggest that successful integration of certain human subunits may be restricted by the broader composition of the complex.

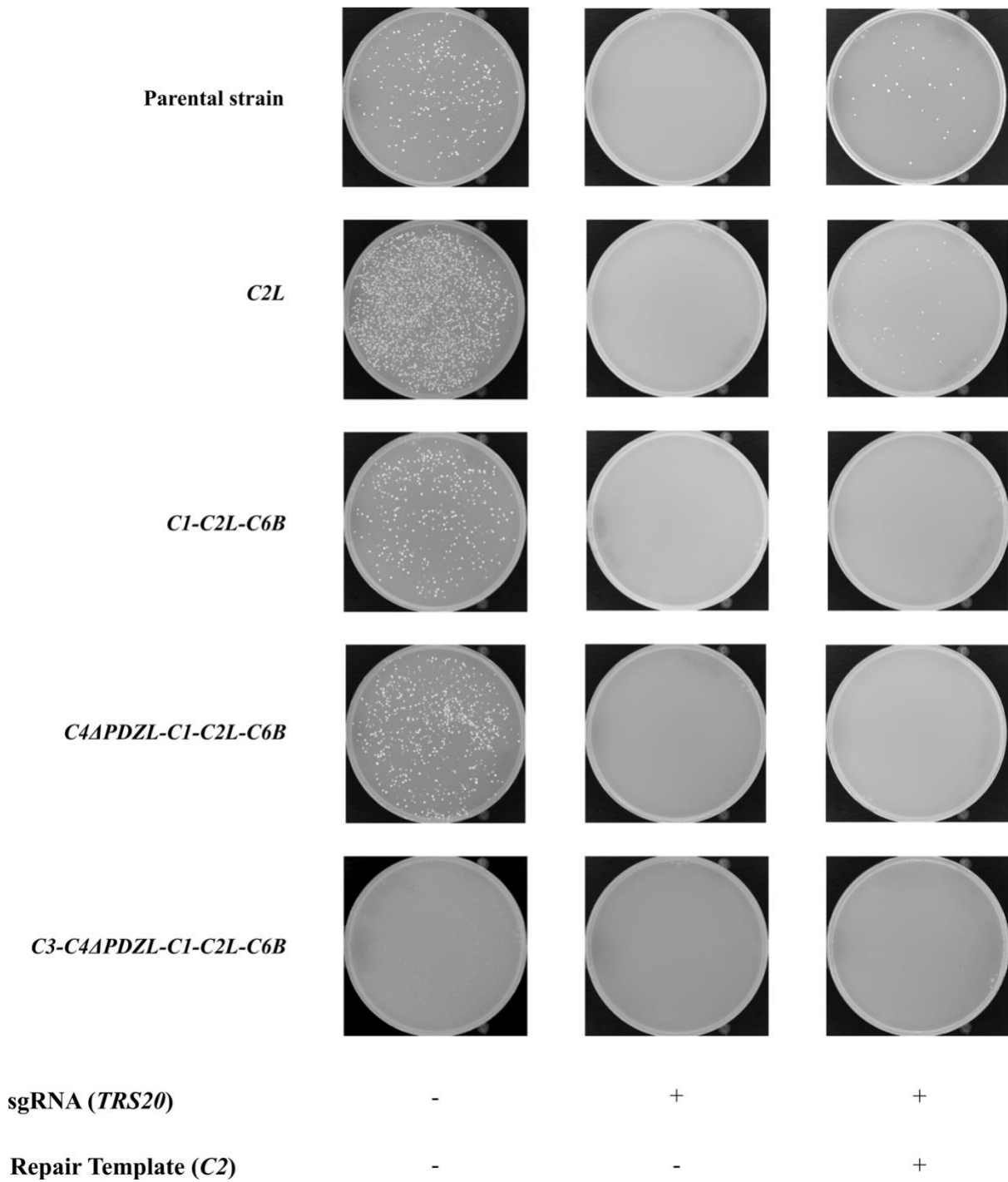


Figure 3.14 Sequential humanization of the C2 Subunit across intermediate humanized TRAPP strain backgrounds using CRISPR-Cas9 Each row represents a yeast strain expressing an increasing number of human TRAPP subunits, as indicated. CRISPR-Cas9 editing targeted the yeast *TRS20* gene (*C2* ortholog), and the human *C2* ORF was used as the repair template. The presence or absence of

sgRNA and repair template is indicated below each column. Transformants were selected on YPD + G418. Colony growth in the +sgRNA/+Repair Template condition indicates successful humanization of *C2*.

3.6 Functional assessment of humanized strains by growth curve analysis

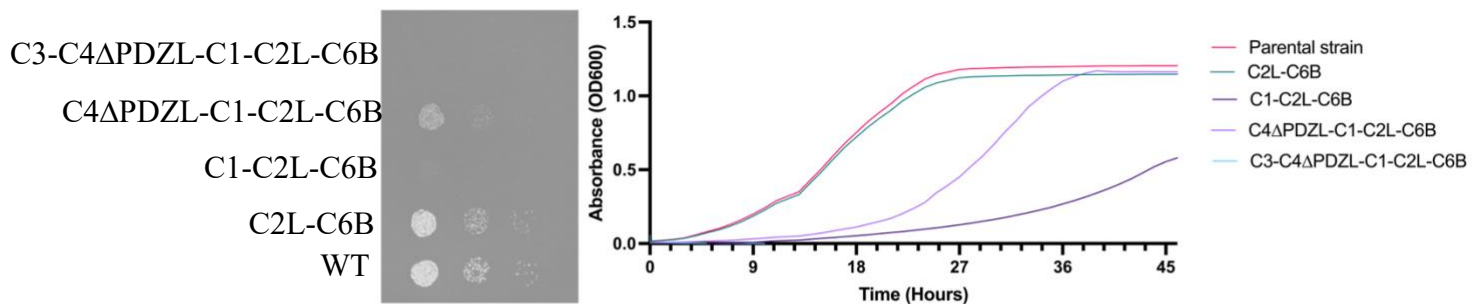
To comprehensively assess the general degree of complementation and function of the humanized TRAPP complexes I measured the fitness of the relevant strains with growth rate analyses. . This approach allowed for a robust comparison of the growth characteristics of partially humanized strains relative to the parental yeast strain and to one another.

At both 25°C and 30°C, the strain harboring humanized *C2L* and *C6B* exhibited growth indistinguishable from that of the parental strain, suggesting that these two human subunits are well tolerated and integrate compatibly within the largely yeast TRAPP complex (**Figure 3.15**). However, when challenged at 37°C, this strain displayed a clear reduction in growth and increased temperature sensitivity, indicating that the stability of these interactions may be compromised under stress. The addition of humanized C1 (C1-*C2L-C6B*) resulted in a strain that grew more poorly than either the parental or the double humanized *C2L-C6B* strains across all three tested temperatures, implying that introduction of C1 has a more destabilizing effect on complex integrity or higher TRAPP requirements under high temperature stress. Interestingly, the strain containing *C4ΔPDZL-C1-C2L-C6B* reached a delayed growth plateau at 25°C and 30°C, but unexpectedly displayed growth comparable to the parental strain at 37°C. This finding suggests that removal of the PDZL domain from C4 may enhance its compatibility with the yeast complex, allowing for improved assembly and function at higher temperatures where other humanized strains falter. In stark contrast, the fully humanized strain containing *C3-C4ΔPDZL-C1-C2L-C6B* failed to grow at both 25°C and 37°C, and exhibited the most impaired growth at 30°C. This severe fitness

defect highlights the cumulative challenge of assembling multiple human subunits within the yeast TRAPP complex, and underscores the limitations imposed by structural incompatibility.

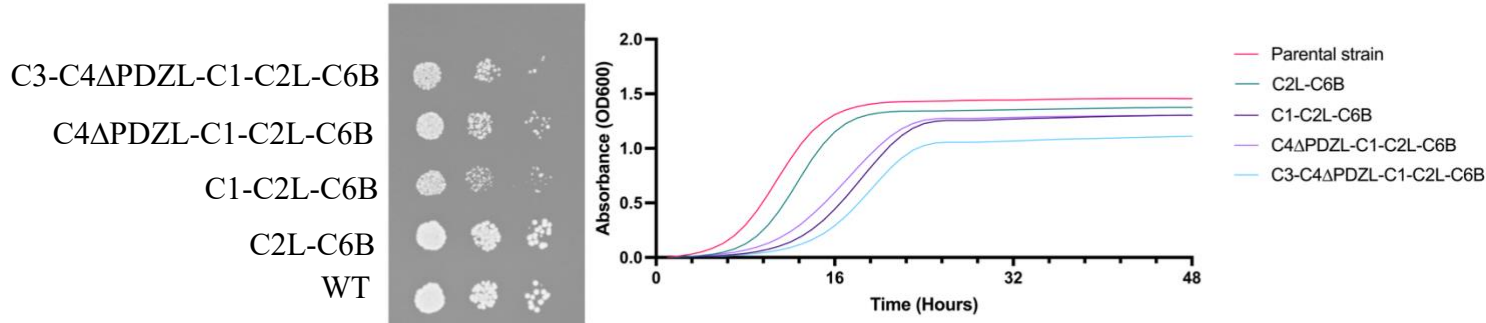
A.

25°C Growth Curve



B.

30°C Growth Curve



C.

37°C Growth Curve

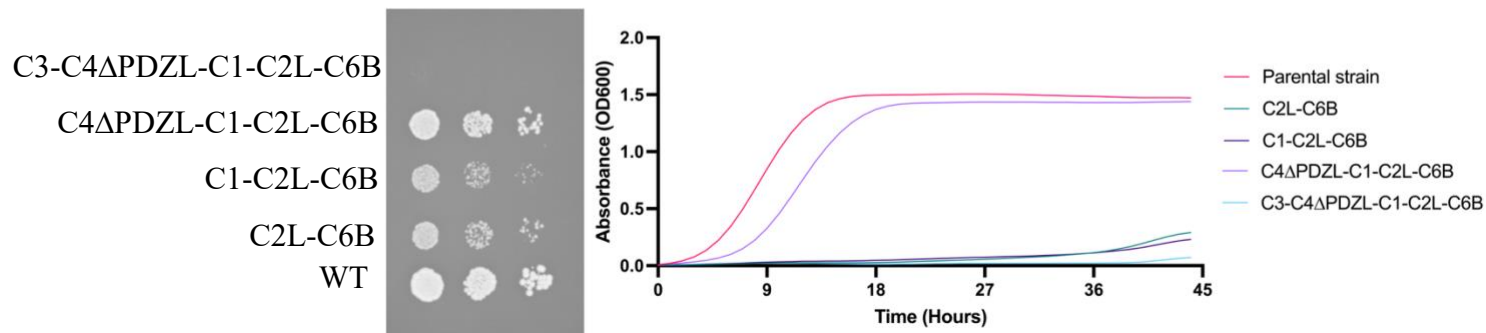


Figure 3.15 Temperature-dependent growth analysis of sequentially humanized TRAPP core strains. (A–C) Yeast growth at 25 °C (A), 30 °C (B), and 37 °C (C). Each panel includes a YPD plate spot assay (left) and the corresponding liquid growth curve (right). For the spot assays, three 10-fold

serial dilutions of each strain (A–E) were plated on YPD and incubated at the indicated temperature. Data were validated using $N = 3$ biological replicates, each with three technical replicates, all showing the same growth pattern. In parallel, liquid cultures of the same strains were grown under identical conditions, and growth was monitored by measuring OD₆₀₀ over time. Strain compositions: A, parental strain; B, C2L–C6B; C, C1–C2L–C6B; D, C4ΔPDZL–C1–C2L–C6B; E, C3–C4ΔPDZL–C1–C2L–C6B.

3.7 Structural mapping and effects of *C3 L131F* mutant

One of the goals of this work was to be able to examine VUS in the absence of human cell samples. To this end, I examined the unpublished C3 mutant L131F using the PHTCC yeast model. This mutant contains a single nucleotide substitution resulting in a missense mutation, changing leucine (L) to phenylalanine (F) at position 131 (L131F) (**Figure 3.16 A**). To predict the structural consequences of this mutation, wild-type (WT) and mutant C3 L131F sequences were modeled and analyzed using PyMOL. Residue interactions were evaluated based on Van der Waals clashes, using a 0.3 Å cutoff (see methods 2.6.1). This analysis illustrates that in the WT structure, residue L131 showed no steric clashes with adjacent residues (**Figure 3.16 B**). However, in the mutant structure, the substitution of L131 to F131 introduced a clash with residue L112 (**Figure 3.16 C**). This clash was consistently identified in both PyMOL and Chimera analyses (data not shown), reinforcing the reliability of this structural prediction. These results suggest that the L131F mutation introduces steric hindrance in the C3 structure, potentially affecting the structural stability or interaction profile within the TRAPP complex.

A.

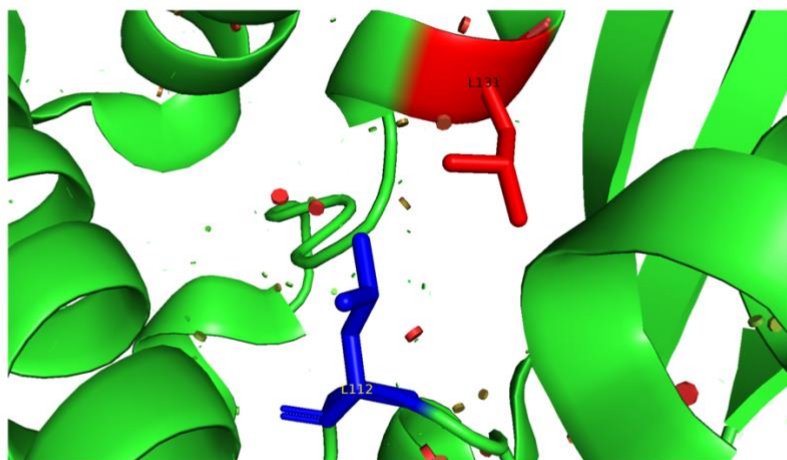
C3 Wild-Type Sequence:

1	MSRQANRGTE	SKKMSSELFT	LTYGALVTQL	CKDYENEDDV	NKQLDKMGFN	IGVRLIEDFL
61	ARSNVGRCHD	FRETADVIAK	VAFKMYLGIT	PSITNWSPAG	DEFSLILENN	PLVDFVELPD
121	NHSSLIYSNL	LCGVLRGALE	MVQMAVEAKF	VQDTLKGDGV	TEIRMRFIRR	IEDNLPAGEE

C3 mutant (L131F) Sequence:

1	MSRQANRGTE	SKKMSSELFT	LTYGALVTQL	CKDYENEDDV	NKQLDKMGFN	IGVRLIEDFL
61	ARSNVGRCHD	FRETADVIAK	VAFKMYLGIT	PSITNWSPAG	DEFSLILENN	P LVDFVELPD
121	NHSSLIYSNL	FCGVLRGALE	MVQMAVEAKF	VQDTLKGDGV	TEIRMRFIRR	IEDNLPAGEE

B.



C.

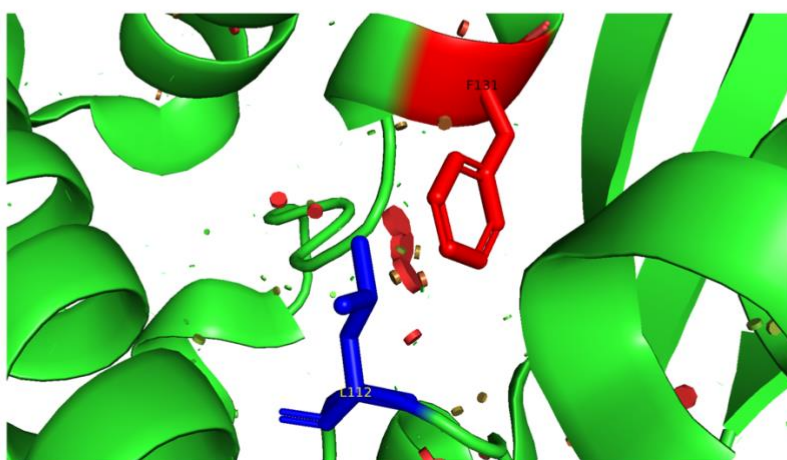


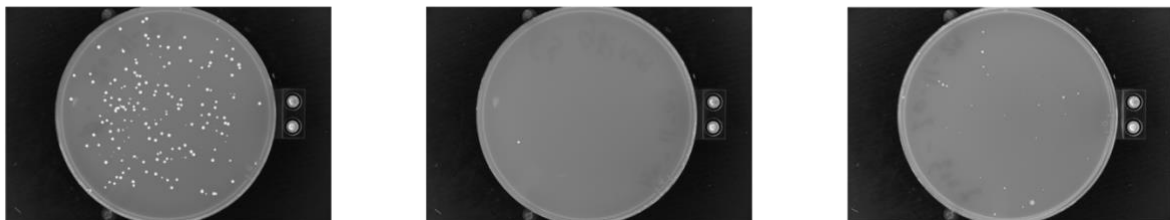
Figure 3.16 Structural and sequence analysis of the C3 L131F mutant and its effects on protein packing (A) Sequence comparison of the C3 wild-type and L131F. The position of the L131F mutation is in red font, while the residue predicted to clash with F131 is highlighted in yellow. (B) Structural model of the wild-type *C3* subunit (green) shows the location of L131 (red) and L112, with no steric clashes observed. (C) In the L131F mutant structure, the mutated F131 residue (red)

introduces a clash with L112, as visualized by close packing and steric overlap (indicated by red discs). Clash analysis was performed using PyMOL and verified with Chimera, confirming that the L131F substitution results in unfavorable interactions with L112, which may destabilize the protein structure.

3.8 Successful humanization of the L131F mutant.

I next used the partially humanized strain (*C4ΔPDZL-C1-C2L-C6B*) to introduce the *C3 L131F* mutation. As shown in **Figure 3.17** the resulting yeast remains viable with this variant. Sanger sequencing (**Figure 3.18**) further confirmed the replacement in a scarless manner. This demonstrates that the *C3 L131F* substitution is tolerated in the context of the humanized TRAPP complex in yeast. Given that our group has previously established the humanized yeast model as a suitable platform for characterizing variants of unknown significance (VUS) (Zykaj et al., 2024), this system can be used to characterize the *C3 L131F* mutant.

A.



sgRNA (Bet3)	-	+	+
Repair Template (L131F)	-	-	+

Figure 3.17 Successful humanization of the L131F in the PHTCC. This figure shows successful humanization of the *C3 L131F* mutant in a strain expressing *C4ΔPDZL-C1-C2L-C6B*. Since this background retains the yeast *BET3* a sgRNA targeting *BET3* was used to introduce a double-stranded break, and a repair template containing the *C3 L131F* mutation was supplied. Colony formation in the

presence of both the sgRNA and the repair template confirms successful incorporation of the *L131F* mutation.

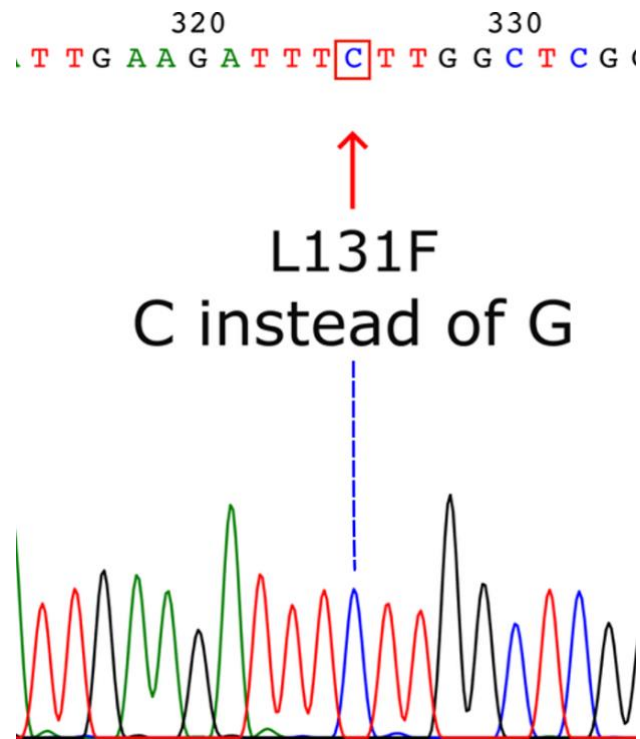


Figure 3.18 Sanger sequencing confirmation of *C3 L131F* mutation in the humanized yeast strain

The chromatogram shows successful integration of the *L131F* missense mutation (C instead of G) in the *C3* ORF, resulting in a leucine-to-phenylalanine substitution at position 131. The boxed base indicates the nucleotide change introduced by CRISPR-Cas9-mediated genome editing.

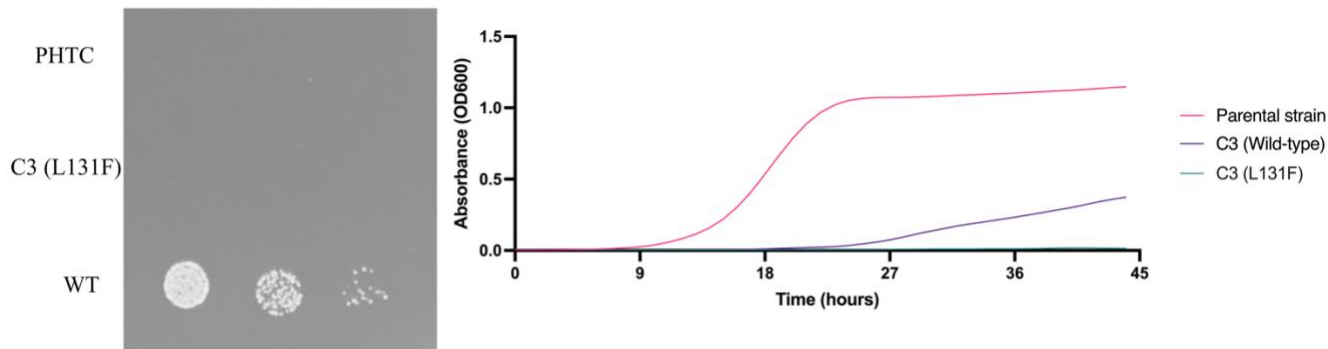
3.9 Characterization of the *L131F C3* mutant

To investigate the functional consequences of the *L131F* mutation in a partially humanized TRAPP core background, I compared the growth of the parental strain, PHTCC and the *C3 L131F* mutant across a

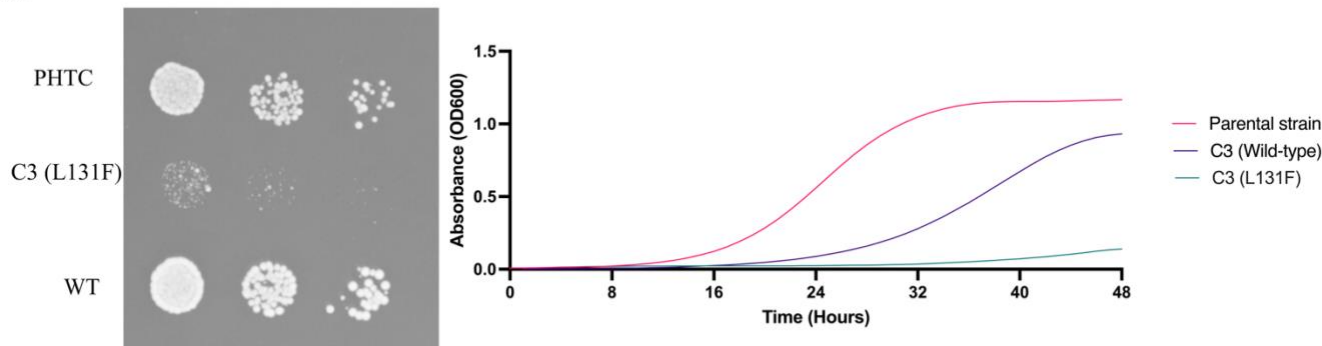
range of temperatures. Growth was assessed both by spot assays and by monitoring liquid culture growth curves at 25°C, 30°C, and 37°C (**Figure 3.19 A–C**).

At 25°C, the parental strain exhibited robust growth in both spot assays and liquid culture, while both the PHTCC and L131F mutant strains showed severely impaired growth, with little to no detectable increase in absorbance (OD₆₀₀) over time. At 30°C, the parental strain again demonstrated the highest growth rate, followed by PHTCC, whereas the L131F mutant strain displayed the poorest growth of the three, showing a significant growth defect in both spot and liquid culture assays. At 37°C, only the parental strain was able to grow; neither PHTCC nor the L131F mutant showed any appreciable growth. These results indicate that C3 L131F further exacerbates the temperature sensitivity and growth defects seen in the partially humanized TRAPP core background. The pronounced growth defect at 30°C suggests that the L131F mutation may significantly compromise the function of C3 in the complex, and highlights its potential pathogenic relevance.

A.



B.



C.

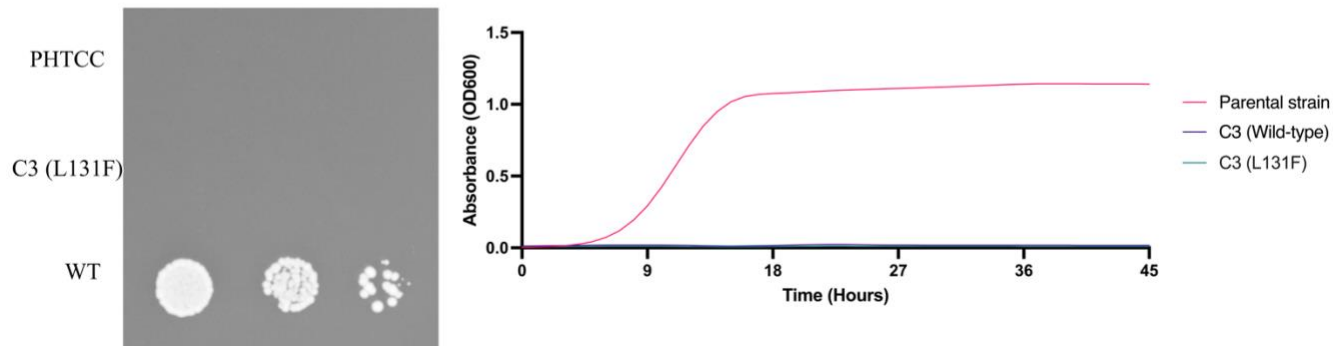


Figure 3.19 Growth analysis of parental, C3 wild-type, and C3 (L131F) mutant strains at different temperatures Panels A, B, and C show serial dilution spot assays (left) and corresponding growth curves (right) at 25 °C, 30 °C, and 37 °C, respectively. Each assay includes the parental strain, a strain containing wild-type C3 in the C3–C4ΔPDZL–C1–C2L–C6B background, and a strain containing the C3 (L131F)

mutant in the same background. Data were validated using $N = 3$ biological replicates, each with three technical replicates, all showing the same growth pattern.

Since TRAPP III is involved in ER-to-Golgi trafficking and TRAPP II functions at the Golgi, I performed a secretion assay to determine whether the C3 L131F mutant exhibits a secretion defect. To do this, I measured the secretion of invertase, encoded by *SUC2*. Invertase expression is repressed in high glucose (2%) but induced in low glucose (0.05%) in the presence of sucrose (2%) (Munn et al., 1999). Yeast cells were grown under both non-inducing and inducing conditions at various temperatures. A *sec18* mutant was included as a control for secretion block.

Invertase activity was assayed in both whole cells (measuring external invertase) and lysed cells (measuring total invertase). This distinction is necessary because O-dianisidine, the substrate used for colorimetric detection, cannot penetrate the yeast spheroplast; thus, activity in intact cells reflects only surface (secreted) invertase, while activity in lysed cells reflects the total enzyme. Based on these measurements, I calculated the percentage of secreted and internal invertase.

Wild-type cells efficiently secreted invertase upon induction, with no significant changes observed at any temperature tested (**Figure 3.20**). As expected, the percentage of secreted invertase in the *sec18* mutant was similar to the control at permissive temperatures but dropped sharply at restrictive temperatures, accompanied by a corresponding increase in internal invertase.

The C3 humanized yeast exhibited a significant increase in internal invertase compared to wild type at all temperatures, indicating a secretion defect. However, the C3 L131F strain showed no additional accumulation of invertase at either temperature relative to the C3 strain. These results indicate that the C3 L131F mutant does not have an enhanced secretion defect compared to the C3 strain.

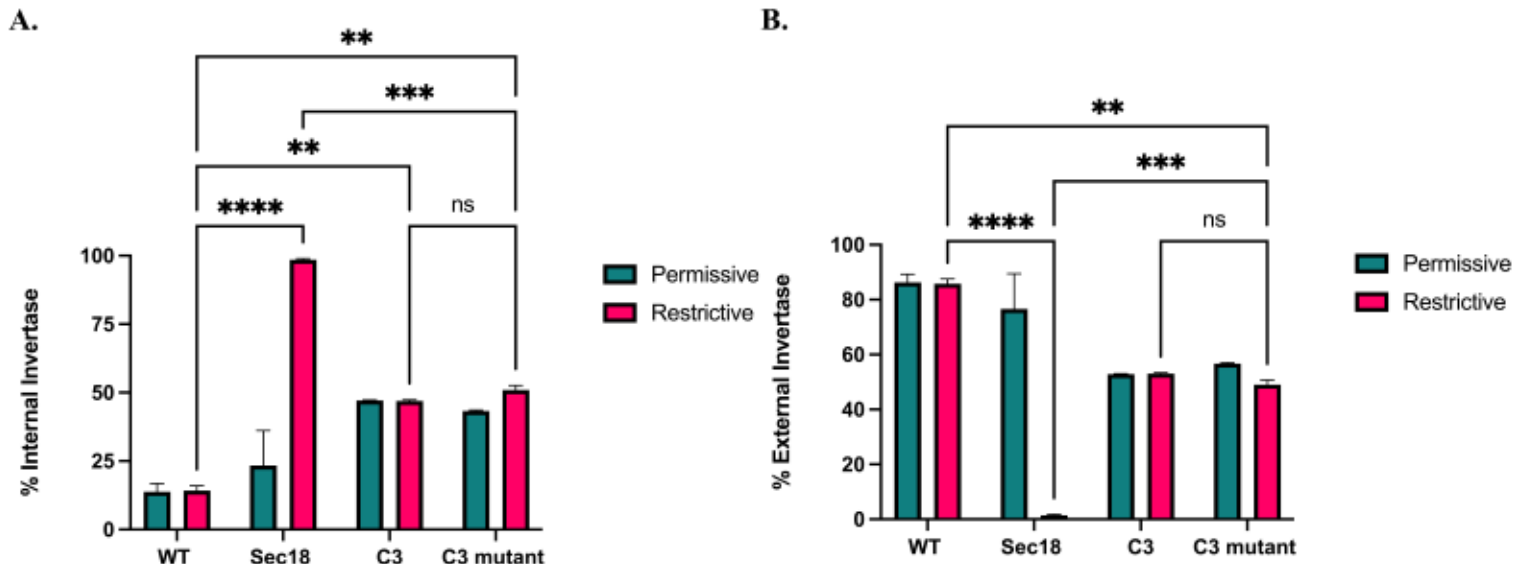


Figure 3.20 Secretion assay to characterize C3 L131F mutant. Yeast cells (wild-type, *sec18*, humanized *C3* and *C3 L131F*) were grown in medium with 0.05% glucose and 2% sucrose to induce expression of the *SUC2* gene that produces the secreted invertase enzyme. Induction was allowed to proceed for 1 h, at which time cells were collected and analyzed before and after lysis to determine percent Internal (A) and External (B) invertase. Percentage Internal was calculated as (lysed cell–whole cell/lysed cell) × 100 and Percentage External was calculated as (whole cell/lysed cell) × 100. N=4 over 2 biological replicates and error bars indicate SEM. Significance was calculated using a one way ANOVA with a Bonferroni post hoc correction. * indicates $p < 0.05$; **** indicates $p < 0.0001$; ns = not significant..

4 Discussion and future work:

This study expands the utility of the humanized yeast model as a platform for investigating multisubunit complexes by enabling the incorporation of previously non-humanizable TRAPP subunits. Using scarless CRISPR-Cas9 editing while preserving endogenous yeast regulatory elements, I achieved native-like expression of several human TRAPP subunits. Building on prior work that validated this model for functional analysis of VUS (Zykaj et al., 2024), I extended its scope to address more challenging targets, such as C3 and a truncated form of C4. The ability to humanize these subunits highlights the flexibility of this model and reinforces its potential for rapid, *in vivo* assessment of TRAPP-related patient variants. However, certain subunits, such as C5, remained refractory to replacement, underscoring the complex interplay of structural compatibility within conserved assemblies.

The successful stepwise replacement of TRAPP subunits such as C6B, C2L, and C1 demonstrates that the yeast system can accommodate multiple human proteins simultaneously, supporting its utility as a platform for progressively assembling multisubunit human complexes (**Figure 3.1**). This is also consistent with large-scale efforts to humanize conserved genes individually (Kachroo et al., 2015). However, not all subunits proved readily replaceable. The inability of human C4 to complement yeast Trs23 under standard conditions underscores a broader challenge in humanizing multisubunit complexes—namely, the need for precise structural compatibility at subunit interfaces. This issue has been observed in other systems as well; for example, it was shown that successful humanization of the proteasome β 2 subunit required appending a yeast-specific C-terminal tail to maintain inter-subunit contacts (Sultana et al., 2023). Analogously, our comparative analysis revealed that human C4 contains a PDZL domain absent in yeast Trs23, potentially disrupting interactions within the TRAPP core. By removing this domain, we generated a truncated variant (C4 Δ PDZL) that restored functionality in yeast, suggesting that domain-specific incompatibilities, rather than broader sequence divergence, can be key

determinants of cross-species replacement success. These findings highlight the importance of structural tailoring in overcoming evolutionary barriers during humanization efforts.

The difficulty of humanizing C3 in isolation, despite its high sequence similarity to yeast Bet3 (Zykaj et al., 2024), suggests that sequence identity alone is insufficient for functional replacement within multisubunit assemblies (**Table 1.1**). This result highlights the importance of structural context and inter-subunit dependencies during humanization. C3 occupies two distinct positions within the TRAPP core, interacting with C4 and C1 on one side and with C5 and C2 on the other, which implies that its successful incorporation may require compatible interfaces with neighboring proteins. Humanization of C3 was only successful when both C1 and the truncated C4 Δ PDZL were present, indicating that interface compatibility with these subunits is both necessary and sufficient for its functional integration. These findings support the idea that successful replacement in conserved complexes often depends on cooperative interactions among subunits, rather than the properties of an individual subunit in isolation. This was also observed in humanization efforts where context dependent compatibility was shown to influence success (Laurent et al., 2016).

Growth phenotypes in humanized yeast do not correlate directly with the number of human subunits present, but rather with the specific compatibility of protein-protein interfaces within the TRAPP complex (**Figure 3.14**). For example, strains containing both C2L and C6B maintain wild-type growth at 25°C and 30°C, indicating functional integration under standard conditions. However, reduced fitness at 37°C suggests that their interactions are destabilized by thermal stress, consistent with marginal interface compatibility. In contrast, the C4 Δ PDZL-containing strain exhibits robust growth across all temperatures, with particularly enhanced growth at 37°C. This supports the conclusion that removal of the PDZL domain improves complex stability and activity enhancement. Structural modeling corroborates this interpretation: inclusion of the PDZL domain introduces steric clashes with C3, whereas its removal eliminates these conflicts (**Figure 3.11**). Conversely, humanization of C3 leads to consistently lower growth at all tested temperatures, underscoring how specific subunit incompatibilities

can compromise complex integrity. More broadly, structural analysis reveals that introducing additional human subunits progressively increases the number of steric clashes within the complex, particularly when neighboring interfaces are not co-adapted (**Figure 3.12 A–E**). These findings reinforce that growth phenotypes in humanized yeast are governed primarily by the structural compatibility of interacting subunits, rather than the extent of humanization itself.

These incompatibilities may explain why C2 can successfully replace Trs20 when humanized alone, yet fails to do so when additional human subunits are present. This observation suggests that while sequence homology is a prerequisite for replacement, structural compatibility within the complex is equally critical. In the case of C2, its ability to integrate functionally depends not only on its own properties, but also on the specific combination and context of its interaction partners. These findings emphasize that humanization of multisubunit assemblies requires consideration of both sequence similarity and structural context, particularly as the number of humanized subunits increases.

The growth phenotypes observed in this study highlight the functional impact of introducing the L131F mutation into the humanized TRAPP complex. Compared to the wild-type humanized strain, the L131F mutant showed a markedly greater growth defect at both 25°C and 30°C, indicating that the substitution impairs viability even under optimal and mildly elevated temperatures (**Figure 3.19**). This pronounced growth defect is consistent with a loss-of-function effect as would be expected for a pathogenic variant. Structural analysis revealed that L131F introduces a steric clash with L112, offering a plausible molecular basis for the observed phenotype (**Figure 3.19**).

To further dissect the functional consequences of the L131F mutation, I performed a secretion assay measuring invertase export from the cell. The results showed that while the humanized C3 strain exhibits a secretion defect relative to wild type, likely reflecting incomplete functional compatibility of the human protein in the yeast cellular context. The introduction of the L131F mutation did not exacerbate this phenotype since the C3 L131F strain did not accumulate additional internal invertase compared to the

humanized C3 strain. Thus, the severe growth defect observed in the L131F mutant does not appear to result from an aggravated secretion impairment.

Given the established roles of the TRAPP complex in both membrane trafficking and autophagy, these findings raise the possibility that the L131F mutation may instead impact autophagy pathways, rather than classical secretion. Further experiments will be required to directly assess autophagic flux in the L131F mutant. More broadly, these results demonstrate the utility of the humanized yeast platform in functionally characterizing specific mutations and suggest that the L131F variant may impair TRAPP complex function in a disease-relevant context. This approach supports the use of humanized yeast models for assessing variants of unknown significance and generating functional evidence to inform clinical interpretation.

Future work will focus on overcoming the remaining barriers to full humanization of the TRAPP core complex in yeast, with particular attention to the subunits C5 and C2 which have resisted replacement in PHTCC. The overlay of Trs31 and C5 show a divergent domain as highlighted (**Figure 4.I**). Future work could focus on either eliminating the entire domain in C5 or to make a domain swap by having the yeast domain in the C5 subunit. Since this divergence is at the extreme amino terminus, such changes would be straightforward. Our work on the C4 Δ PDZL shows that increasing homology between the yeast and human subunit would increase the chance of successful replacement. So swapping the highlighted C5 domain might be necessary and sufficient for the replacement of Trs31 with C5. For the C2 subunit, replacing the subunits sequentially starting from C2 and following the same sequential humanization steps as the ones presented in this study could allow the incorporation of C2 in a fully humanized TRAPP core. Structural studies using tools like cryo-EM for experimental visualization will be critical to elucidate the precise determinants of interface compatibility and to guide rational engineering of human-yeast hybrid complexes.

A.

```
1 MEARFTRGKS 11 ALLERALARP 21 RTEVSLSAFA 31 LLFSELVQHC 41 QSRVFSVAEL 51 QSRLAALGRQ  
61 VGARVLDALV 71 AREKGARRET 81 KVLGALLFVK 91 GAVWKALFGK 101 EADKLEQAND 111 DARTFYIIER  
121 EPLINTYISV 131 PKENSTLNCA 141 SFTAGIVEAV 151 LTHSGFPAK 161 VTAHWHKGTT 171 LMIKFEEAVI  
181ARDRALEQQ
```

B.



Figure 4.1 C5 and Trs31 Overlay (A) The amino acid sequence of human C5 is shown. Regions that are highly divergent from the yeast sequence are highlighted in yellow. (B) Structural overlay of human C5 (dark purple) and yeast Trs31 (light purple). The region of human C5 corresponding to the highlighted divergent sequence in panel A is colored green. This highlights the location and structure of the divergent domain in the context of the full-length protein.

Moreover, complex-specific subunits are valuable targets for humanization, though they present unique challenges. Notably, C8 (4,308 bp), C9 (3,741 bp), C10 (3,780 bp) and C13 (1,257 bp), are among the largest TRAPP subunits, making cloning and scarless replacement technically demanding. Nevertheless, the successful humanization of similarly large complexes has been demonstrated. For example, full humanization of the glycolytic pathway in yeast was achieved, seamlessly integrating and expressing multiple human genes (including those approaching 3 kb) in an essential metabolic pathway (Laurent et

al., 2016). Incorporating these complex-specific subunits will facilitate the characterization of additional mutants, increasing the model's relevance for studying patient-derived mutations.

Among these subunits, *C8* presents a distinct case due to its ambiguous orthology to the yeast subunit *TRS85*. While both *C8* and *Trs85* are unique to the TRAPPIII complex and are functionally involved in autophagy-related trafficking, they exhibit low sequence conservation and marked differences in size, with *C8* (~160 kDa) being significantly larger than *Trs85* (~80.5 kDa). This has led to *C8* being described as a functional analogue rather than a strict orthologue of *Trs85* (Hoffman-Sommer et al., 2025; Tan et al., 2013). Structural studies support their analogous roles in binding to the core complex and recruiting TRAPPIII-specific cargo, but the lack of direct homology introduces uncertainty in establishing a one-to-one replacement. As such, the humanization of *C8* may require additional modification to confirm proper integration and function in the yeast TRAPPIII architecture.

Finally, it is also important to note that the successful integration of TRAPPC8 and TRAPPC9 may require the prior incorporation of TRAPPC2, which acts as an adaptor for both subunits (Zong et al., 2011), further emphasizing the need for a staged and modular approach to humanizing the TRAPP complex.

Functionally, the humanized yeast model offers an ideal platform for high throughput assessment of a wide range of variants introduced by site directed mutagenesis, enabling systematic evaluation of their effects on complex assembly, protein stability, and cellular growth. Beyond genetic analysis, future studies can also employ biophysical methods such as circular dichroism (CD) spectroscopy to directly assess the folding and thermal stability of purified humanized or mutant TRAPP subunits and complexes, providing a mechanistic link between structure, function, and cellular phenotype. Finally, integrating these approaches with collaborative efforts in clinical genetics may further establish humanized yeast as a versatile and translationally relevant tool for interpreting VUS in TRAPP related disorders.

Overall this thesis establishes a translational workflow that begins with the identification of patients with rare, undiagnosed TRAPPopathies and proceeds to modeling patient-derived TRAPP variants in a

humanized yeast platform (**Figure 4.1**). Using stepwise CRISPR-based gene replacement, I reconstructed the TRAPP core with human orthologs and introduced clinically relevant mutations to systematically assess their effects on cellular viability and function. This approach is particularly significant because TRAPPopathies are rare diseases, making patient recruitment difficult, and obtaining primary cells is invasive and often impractical. By leveraging yeast as a model, this platform enables rapid, high-throughput functional interpretation of variants—distinguishing between pathogenic alleles, such as C3 L131F, which cause clear growth defects, and those compatible with normal function. However, the main limitation is that not all subunits are humanized, potentially excluding some mutations from analysis, and complex specific subunits such as *C11* and *C12* do not have homologues in yeast, so they cannot be humanized. Despite these challenges, this workflow provides a practical and scalable bridge between clinical genomics and experimental biology, offering a valuable tool for variant interpretation and advancing rare disease diagnosis, ultimately helping to improve patient care and quality of life.

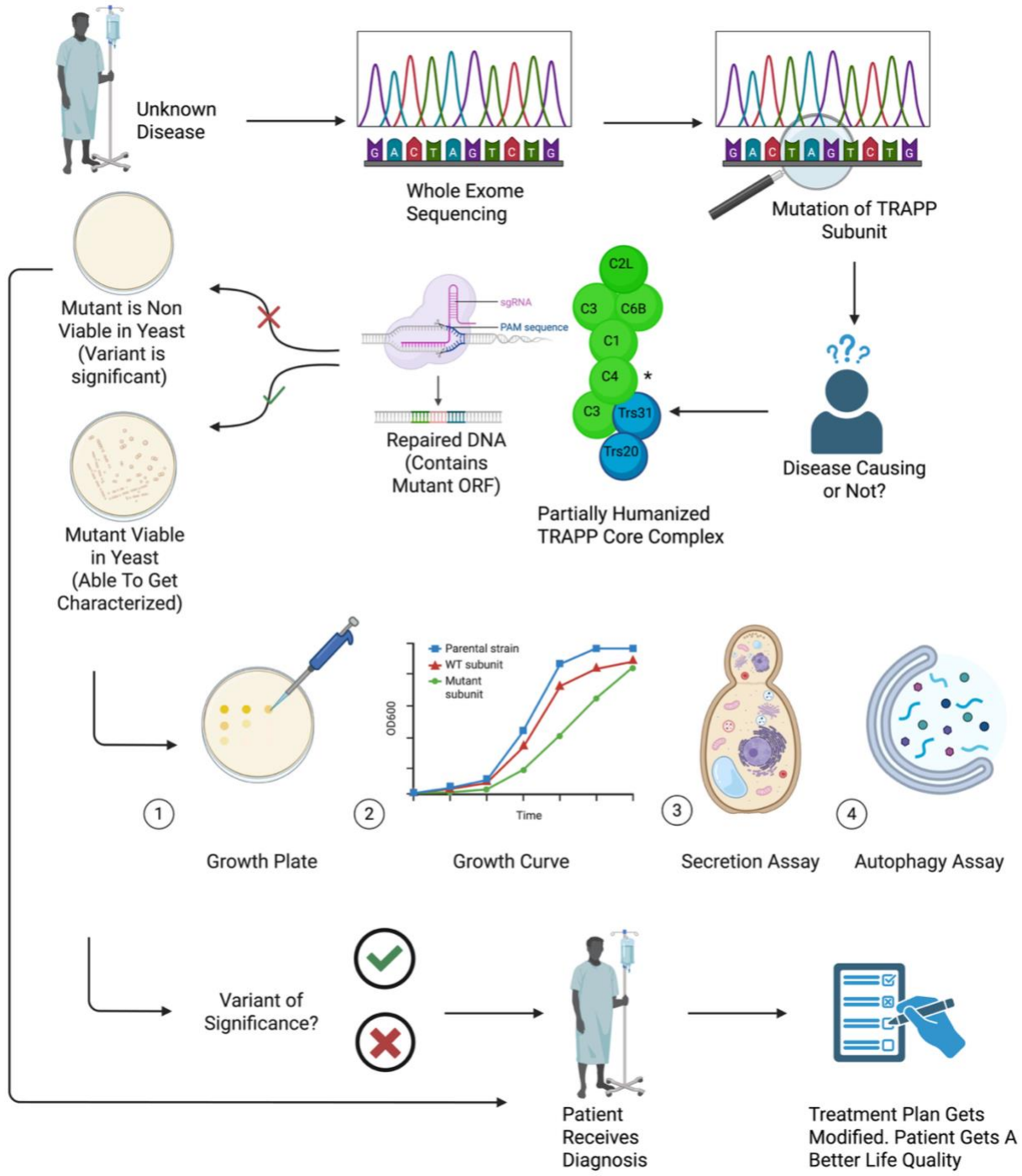


Figure 4.2 Graphical abstract showing significance of study The schematic illustrates the translational pipeline developed in this thesis for assessing the pathogenicity of TRAPP complex variants identified in patients with rare, undiagnosed disease. Clinical sequencing (whole exome) identifies mutations in TRAPP subunits of uncertain significance. To determine pathogenicity, variants are introduced into a humanized TRAPP core complex in *Saccharomyces cerevisiae* using CRISPR-based gene replacement.

Mutant yeast strains are evaluated for viability: non-viable mutants cannot be characterized further, while viable strains undergo functional assessment. Key assays include (1) growth plate analysis, (2) growth curve measurement, (3) secretion assays, and (4) autophagy assays to evaluate cellular consequences of the mutation. Results are interpreted to determine if the variant is pathogenic. This information supports clinical diagnosis and guides patient management, with the goal of improving patient care and quality of life. This workflow is particularly valuable for rare diseases where patient cells are difficult to obtain.

5 References:

- Abt, T. D., Souffriau, B., Foulquie-Moreno, M. R., Duitama, J., & Thevelein, J. M. (2016). Genomic saturation mutagenesis and polygenic analysis identify novel yeast genes affecting ethyl acetate production, a non-selectable polygenic trait. *Microb Cell*, 3(4), 159-175. <https://doi.org/10.15698/mic2016.04.491>
- Almousa, H., Lewis, S. A., Bakhtiari, S., Nordlie, S. H., Pagnozzi, A., Magee, H., Efthymiou, S., Heim, J. A., Cornejo, P., Zaki, M. S., Anwar, N., Maqbool, S., Rahman, F., Neilson, D. E., Vemuri, A., Jin, S. C., Yang, X. R., Heidari, A., van Gassen, K.,...Kruer, M. C. (2024). TRAPPC6B biallelic variants cause a neurodevelopmental disorder with TRAPP II and trafficking disruptions. *Brain*, 147(1), 311-324. <https://doi.org/10.1093/brain/awad301>
- Amin, M., Vignal, C., Eltaraifee, E., Mohammed, I. N., Hamed, A. A. A., Elseed, M. A., Babai, A., Elbadi, I., Mustafa, D., Abubaker, R., Mustafa, M., Drunat, S., Elsayed, L. E. O., Ahmed, A. E., Boespflug-Tanguy, O., & Dorboz, I. (2022). A novel homozygous mutation in TRAPPC9 gene causing autosomal recessive non-syndromic intellectual disability. *BMC Med Genomics*, 15(1), 236. <https://doi.org/10.1186/s12920-022-01354-1>
- Baldridge, D., Wangler, M. F., Bowman, A. N., Yamamoto, S., Undiagnosed Diseases, N., Schedl, T., Pak, S. C., Postlethwait, J. H., Shin, J., Solnica-Krezel, L., Bellen, H. J., & Westerfield, M. (2021). Model organisms contribute to diagnosis and discovery in the undiagnosed diseases network: current state and a future vision. *Orphanet J Rare Dis*, 16(1), 206. <https://doi.org/10.1186/s13023-021-01839-9>
- Bogershausen, N., Shahrzad, N., Chong, J. X., von Kleist-Retzow, J. C., Stanga, D., Li, Y., Bernier, F. P., Loucks, C. M., Wirth, R., Puffenberger, E. G., Hegele, R. A., Schreml, J., Lapointe, G., Keupp, K., Brett, C. L., Anderson, R., Hahn, A., Innes, A. M., Suchowersky, O.,...Lamont, R. E. (2013). Recessive TRAPPC11 mutations cause a disease spectrum of limb girdle muscular dystrophy and

myopathy with movement disorder and intellectual disability. *Am J Hum Genet*, 93(1), 181-190.

<https://doi.org/10.1016/j.ajhg.2013.05.028>

Boonekamp, F. J., Knibbe, E., Vieira-Lara, M. A., Wijsman, M., Luttik, M. A. H., van Eunen, K., Ridder, M. D., Bron, R., Almonacid Suarez, A. M., van Rijn, P., Wolters, J. C., Pabst, M., Daran, J. M., Bakker, B. M., & Daran-Lapujade, P. (2022). Full humanization of the glycolytic pathway in *Saccharomyces cerevisiae*. *Cell Rep*, 39(13), 111010.

<https://doi.org/10.1016/j.celrep.2022.111010>

Brunet, S., Noueihed, B., Shahrzad, N., Saint-Dic, D., Hasaj, B., Guan, T. L., Moores, A., Barlowe, C., & Sacher, M. (2012). The SMS domain of Trs23p is responsible for the in vitro appearance of the TRAPP I complex in *Saccharomyces cerevisiae*. *Cell Logist.*, 2(1), 28-42.

<http://www.ncbi.nlm.nih.gov/pubmed/22645708> (Not in File)

Cai, H., Yu, S., Menon, S., Cai, Y., Lazarova, D., Fu, C., Reinisch, K., Hay, J. C., & Ferro-Novick, S. (2007). TRAPPI tethers COPII vesicles by binding the coat subunit Sec23. *Nature*, 445(7130), 941-944. <http://www.ncbi.nlm.nih.gov/pubmed/17287728> (Not in File)

Cannon, S., Williams, M., Gunning, A. C., & Wright, C. F. (2023). Evaluation of in silico pathogenicity prediction tools for the classification of small in-frame indels. *BMC Med Genomics*, 16(1), 36. <https://doi.org/10.1186/s12920-023-01454-6>

Chiari, R., Foury, F., De Plaen, E., Baurain, J. F., Thonnard, J., & Coulie, P. G. (1999). Two antigens recognized by autologous cytolytic T lymphocytes on a melanoma result from a single point mutation in an essential housekeeping gene. *Cancer Res*, 59(22), 5785-5792. <https://www.ncbi.nlm.nih.gov/pubmed/10582700>

Choi, C., Davey, M., Schluter, C., Pandher, P., Fang, Y., Foster, L. J., & Conibear, E. (2011). Organization and assembly of the TRAPPII complex. *Traffic*, 12(6), 715-725. <http://www.ncbi.nlm.nih.gov/pubmed/21453443> (Not in File)

Fields, S., & Johnston, M. (2005). Cell biology. Whither model organism research? *Science*, 307(5717), 1885-1886. <https://doi.org/10.1126/science.1108872>

Galindo, A., & Munro, S. (2023). The TRAPP complexes: oligomeric exchange factors that activate the small GTPases Rab1 and Rab11. *FEBS Lett.*, 597(6), 734-749. <https://doi.org/10.1002/1873-3468.14553>

Gavin, A. C., Bosche, M., Krause, R., Grandi, P., Marzioch, M., Bauer, A., Schultz, J., Rick, J. M., Michon, A. M., Cruciat, C. M., Remor, M., Hofert, C., Schelder, M., Brajenovic, M., Ruffner, H., Merino, A., Klein, K., Hudak, M., Dickson, D.,...Superti-Furga, G. (2002). Functional organization of the yeast proteome by systematic analysis of protein complexes. *Nature*, 415(6868), 141-147. <http://www.ncbi.nlm.nih.gov/pubmed/11805826> (Not in File)

Hall, R., Sawant, V., Gu, J., Sikora, T., Rollo, B., Velasco, S., Kim, J., Segev, N., Christodoulou, J., & Van Bergen, N. J. (2024). TRAPPopathies: Severe Multisystem Disorders Caused by Variants in Genes of the Transport Protein Particle (TRAPP) Complexes. *Int J Mol Sci*, 25(24). <https://doi.org/10.3390/ijms252413329>

Hamza, A., Tamppere, E., Kofoed, M., Keong, C., Chiang, J., Giaever, G., Nislow, C., & Hieter, P. (2015). Complementation of Yeast Genes with Human Genes as an Experimental Platform for Functional Testing of Human Genetic Variants. *Genetics*, 201(3), 1263-1274. <https://doi.org/10.1534/genetics.115.181099>

Hoffman-Sommer, M., Pilka, N., Anielska-Mazur, A., Nowakowska, J., Kozieradzka-Kiszkurno, M., Paczkowski, C., Jemiola-Rzeminska, M., Steczkiewicz, K., Dagdas, Y., & Swiezewska, E. (2025). The TRAPPC8/TRS85 subunit of the Arabidopsis TRAPPIII tethering complex regulates endoplasmic reticulum function and autophagy. *Plant Physiol*, 197(3). <https://doi.org/10.1093/plphys/kiaf042>

Kachroo, A. H., Laurent, J. M., Yellman, C. M., Meyer, A. G., Wilke, C. O., & Marcotte, E. M. (2015).

Evolution. Systematic humanization of yeast genes reveals conserved functions and genetic modularity. *Science*, 348(6237), 921-925. <https://doi.org/10.1126/science.aaa0769>

Kachroo, A. H., Vandeloo, M., Greco, B. M., & Abdullah, M. (2022). Humanized yeast to model human biology, disease and evolution. *Dis Model Mech*, 15(6). <https://doi.org/10.1242/dmm.049309>

Kaiser, C. A., & Schekman, R. (1990). Distinct sets of SEC genes govern transport vesicle formation and fusion early in the secretory pathway. *Cell*, 61(4), 723-733. [https://doi.org/10.1016/0092-8674\(90\)90483-u](https://doi.org/10.1016/0092-8674(90)90483-u)

Kataoka, T., Broek, D., & Wigler, M. (1985). DNA sequence and characterization of the *S. cerevisiae* gene encoding adenylate cyclase. *Cell*, 43(2 Pt 1), 493-505. [https://doi.org/10.1016/0092-8674\(85\)90179-5](https://doi.org/10.1016/0092-8674(85)90179-5)

Kim, J. J., Lipatova, Z., & Segev, N. (2016). TRAPP Complexes in Secretion and Autophagy. *Front Cell Dev Biol*, 4, 20. <https://doi.org/10.3389/fcell.2016.00020>

Kim, Y. G., Raunser, S., Munger, C., Wagner, J., Song, Y. L., Cygler, M., Walz, T., Oh, B. H., & Sacher, M. (2006). The architecture of the multisubunit TRAPP I complex suggests a model for vesicle tethering. *Cell*, 127(4), 817-830. <http://www.ncbi.nlm.nih.gov/pubmed/17110339> (Not in File)

Kimura, H., Paranal, R. M., Nanda, N., Wood, L. D., Eshleman, J. R., Hruban, R. H., Goggins, M. G., Klein, A. P., Familial Pancreatic Cancer Genome Sequencing, P., & Roberts, N. J. (2022). Functional CDKN2A assay identifies frequent deleterious alleles misclassified as variants of uncertain significance. *Elife*, 11. <https://doi.org/10.7554/eLife.71137>

Laurent, J. M., Young, J. H., Kachroo, A. H., & Marcotte, E. M. (2016). Efforts to make and apply humanized yeast. *Brief Funct Genomics*, 15(2), 155-163. <https://doi.org/10.1093/bfgp/elv041>

Lynch-Day, M. A., Bhandari, D., Menon, S., Huang, J., Cai, H., Bartholomew, C. R., Brumell, J. H., Ferro-Novick, S., & Klionsky, D. J. (2010). Trs85 directs a Ypt1 GEF, TRAPPIII, to the

phagophore to promote autophagy. *Proc.Natl.Acad.Sci.U.S.A.*, 107(17), 7811-7816.

<http://www.ncbi.nlm.nih.gov/pubmed/20375281> (Not in File)

Menon, S., Cai, H., Lu, H., Dong, G., Cai, Y., Reinisch, K., & Ferro-Novick, S. (2006). mBET3 is required for the organization of the TRAPP complexes. *Biochem Biophys Res Commun*, 350(3), 669-677. <https://doi.org/10.1016/j.bbrc.2006.09.096>

Milev, M. P., Grout, M. E., Saint-Dic, D., Cheng, Y. H., Glass, I. A., Hale, C. J., Hanna, D. S., Dorschner, M. O., Prematilake, K., Shaag, A., Elpeleg, O., Sacher, M., Doherty, D., & Edvardson, S. (2017). Mutations in TRAPPC12 Manifest in Progressive Childhood Encephalopathy and Golgi Dysfunction. *Am.J.Hum.Genet.*, 101(2), 291-299.

<http://www.ncbi.nlm.nih.gov/pubmed/28777934> (Not in File)

Montpetit, B., & Conibear, E. (2009). Identification of the novel TRAPP associated protein Tca17. *Traffic*, 10(6), 713-723. <http://www.ncbi.nlm.nih.gov/pubmed/19220810> (Not in File)

Morozova, N., Liang, Y., Tokarev, A. A., Chen, S. H., Cox, R., Andrejic, J., Lipatova, Z., Sciorra, V. A., Emr, S. D., & Segev, N. (2006). TRAPPII subunits are required for the specificity switch of a Ypt-Rab GEF. *Nat.Cell Biol.*, 8(11), 1263-1269.

<http://www.ncbi.nlm.nih.gov/pubmed/17041589> (Not in File)

Munn, A. L., Heese-Peck, A., Stevenson, B. J., Pichler, H., & Riezman, H. (1999). Specific sterols required for the internalization step of endocytosis in yeast. *Mol Biol Cell*, 10(11), 3943-3957. <https://doi.org/10.1091/mbc.10.11.3943>

Olafsson, G., Haase, M. A. B., & Boeke, J. D. (2023). Humanization reveals pervasive incompatibility of yeast and human kinetochore components. *G3 (Bethesda)*, 14(1). <https://doi.org/10.1093/g3journal/jkad260>

Riedel, F., Galindo, A., Muschalik, N., & Munro, S. (2018). The two TRAPP complexes of metazoans have distinct roles and act on different Rab GTPases. *J Cell Biol*, 217(2), 601-617. <https://doi.org/10.1083/jcb.201705068>

Sacher, M., Barrowman, J., Wang, W., Horecka, J., Zhang, Y., Pypaert, M., & Ferro-Novick, S. (2001).

TRAPP I implicated in the specificity of tethering in ER-to-Golgi transport. *Mol.Cell*, 7(2), 433-442. <http://www.ncbi.nlm.nih.gov/pubmed/11239471> (Not in File)

Sacher, M., & Ferro-Novick, S. (2001). Purification of TRAPP from *Saccharomyces cerevisiae* and identification of its mammalian counterpart. *Methods Enzymol.*, 329, 234-241. <http://www.ncbi.nlm.nih.gov/pubmed/11210539> (Not in File)

Sacher, M., Jiang, Y., Barrowman, J., Scarpa, A., Burston, J., Zhang, L., Schielitz, D., Yates, J. R., III, Abeliovich, H., & Ferro-Novick, S. (1998). TRAPP, a highly conserved novel complex on the cis-Golgi that mediates vesicle docking and fusion. *EMBO J.*, 17(9), 2494-2503. <http://www.ncbi.nlm.nih.gov/pubmed/9564032> (Not in File)

Sacher, M., Shahrzad, N., Kamel, H., & Milev, M. P. (2019). TRAPPopathies: An emerging set of disorders linked to variations in the genes encoding transport protein particle (TRAPP)-associated proteins. *Traffic*, 20(1), 5-26. <https://doi.org/10.1111/tra.12615>

Satam, H., Joshi, K., Mangrolia, U., Waghoo, S., Zaidi, G., Rawool, S., Thakare, R. P., Banday, S., Mishra, A. K., Das, G., & Malonia, S. K. (2023). Next-Generation Sequencing Technology: Current Trends and Advancements. *Biology (Basel)*, 12(7). <https://doi.org/10.3390/biology12070997>

Scrivens, P. J., Shahrzad, N., Moores, A., Morin, A., Brunet, S., & Sacher, M. (2009). TRAPPC2L is a novel, highly conserved TRAPP-interacting protein. *Traffic*, 10(6), 724-736. <http://www.ncbi.nlm.nih.gov/pubmed/19416478> (Not in File)

Shirahama-Noda, K., Kira, S., Yoshimori, T., & Noda, T. (2013). TRAPPIII is responsible for vesicular transport from early endosomes to Golgi, facilitating Atg9 cycling in autophagy. *J.Cell Sci.*, 126(Pt 21), 4963-4973. <http://www.ncbi.nlm.nih.gov/pubmed/23986483> (Not in File)

Somanadhan, S., Nicholson, E., Dorris, E., Brinkley, A., Kennan, A., Treacy, E., Atif, A., Ennis, S., McGrath, V., Mitchell, D., O'Sullivan, G., Power, J., Lawlor, A., Harkin, P., Lynch, S. A., Watt,

- P., Daly, A., Donnelly, S., & Kroll, T. (2020). Rare Disease Research Partnership (RAinDRoP): a collaborative approach to identify research priorities for rare diseases in Ireland. *HRB Open Res*, 3, 13. <https://doi.org/10.12688/hrbopenres.13017.2>
- Sultana, S., Abdullah, M., Li, J., Hochstrasser, M., & Kachroo, A. H. (2023). Species-specific protein-protein interactions govern the humanization of the 20S proteasome in yeast. *Genetics*, 225(1). <https://doi.org/10.1093/genetics/iyad117>
- Tan, D., Cai, Y., Wang, J., Zhang, J., Menon, S., Chou, H. T., Ferro-Novick, S., Reinisch, K. M., & Walz, T. (2013). The EM structure of the TRAPPIII complex leads to the identification of a requirement for COPII vesicles on the macroautophagy pathway. *Proc.Natl.Acad.Sci.U.S.A.*, 110(48), 19432-19437. <http://www.ncbi.nlm.nih.gov/pubmed/24218626> (Not in File)
- Thomas, L. L., & Fromme, J. C. (2016). GTPase cross talk regulates TRAPPII activation of Rab11 homologues during vesicle biogenesis. *J.Cell Biol.*, 215(4), 499-513. <http://www.ncbi.nlm.nih.gov/pubmed/27872253> (Not in File)
- Thomas, L. L., Joiner, A. M. N., & Fromme, J. C. (2018). The TRAPPIII complex activates the GTPase Ypt1 (Rab1) in the secretory pathway. *J Cell Biol*, 217(1), 283-298. <https://doi.org/10.1083/jcb.201705214>
- Tiller, G. E., Hannig, V. L., Dozier, D., Carrel, L., Trevarthen, K. C., Wilcox, W. R., Mundlos, S., Haines, J. L., Gedeon, A. K., & Gecz, J. (2001). A recurrent RNA-splicing mutation in the SEDL gene causes X-linked spondyloepiphyseal dysplasia tarda. *Am.J.Hum.Genet.*, 68(6), 1398-1407. <http://www.ncbi.nlm.nih.gov/pubmed/11326333> (Not in File)
- Timmermans, S., Tietbohl, C. & Skaperdas, E. (2017). Narrating uncertainty: Variants of uncertain significance (VUS) in clinical exome sequencing. *BioSocieties*, 12, 439–458 <https://doi.org/10.1057/s41292-016-0020-5>

Tokarev, A. A., Taussig, D., Sundaram, G., Lipatova, Z., Liang, Y., Mulholland, J. W., & Segev, N. (2009). TRAPP II complex assembly requires Trs33 or Trs65. *Traffic*, 10(12), 1831-1844. <https://doi.org/10.1111/j.1600-0854.2009.00988.x>

Twigg, S. R. F., Greene, N. D. E., Henderson, D. J., Mill, P., & Liu, K. J. (2025). The power of mouse models in the diagnostic odyssey of patients with rare congenital anomalies. *Mamm Genome*, 36(2), 354-362. <https://doi.org/10.1007/s00335-025-10114-2>

Van Bergen, N. J., Guo, Y., Al-Deri, N., Lipatova, Z., Stanga, D., Zhao, S., Murtazina, R., Gyurkovska, V., Pehlivan, D., Mitani, T., Gezdirici, A., Antony, J., Collins, F., Willis, M. J. H., Coban Akdemir, Z. H., Liu, P., Punetha, J., Hunter, J. V., Jhangiani, S. N.,...Christodoulou, J. (2020). Deficiencies in vesicular transport mediated by TRAPPC4 are associated with severe syndromic intellectual disability. *Brain*, 143(1), 112-130. <https://doi.org/10.1093/brain/awz374>

Wang, W., Sacher, M., & Ferro-Novick, S. (2000). TRAPP stimulates guanine nucleotide exchange on Ypt1p. *J.Cell Biol.*, 151(2), 289-296. <http://www.ncbi.nlm.nih.gov/pubmed/11038176> (Not in File)

Wangler, M. F., Yamamoto, S., Chao, H. T., Posey, J. E., Westerfield, M., Postlethwait, J., Members of the Undiagnosed Diseases, N., Hieter, P., Boycott, K. M., Campeau, P. M., & Bellen, H. J. (2017). Model Organisms Facilitate Rare Disease Diagnosis and Therapeutic Research. *Genetics*, 207(1), 9-27. <https://doi.org/10.1534/genetics.117.203067>

Westlake, C. J., Baye, L. M., Nachury, M. V., Wright, K. J., Ervin, K. E., Phu, L., Chalouni, C., Beck, J. S., Kirkpatrick, D. S., Slusarski, D. C., Sheffield, V. C., Scheller, R. H., & Jackson, P. K. (2011). Primary cilia membrane assembly is initiated by Rab11 and transport protein particle II (TRAPPII) complex-dependent trafficking of Rabin8 to the centrosome. *Proc.Natl.Acad.Sci.U.S.A.*, 108(7), 2759-2764. <http://www.ncbi.nlm.nih.gov/pubmed/21273506> (Not in File)

Wu, S., Qi, L., Chen, H., Zhang, K., He, J., Guo, X., Shen, L., Zhou, Y., Zhong, X., Zheng, S., Zhou, J., & Chen, Y. (2022). Functional assessment of missense variants of uncertain significance in the cancer susceptibility gene PALB2. *NPJ Breast Cancer*, 8(1), 86. <https://doi.org/10.1038/s41523-022-00454-6>

Yamasaki, A., Menon, S., Yu, S., Barrowman, J., Meerloo, T., Oorschot, V., Klumperman, J., Satoh, A., & Ferro-Novick, S. (2009). mTrs130 is a component of a mammalian TRAPPII complex, a Rab1 GEF that binds to COPI-coated vesicles. *Mol.Biol.Cell*, 20(19), 4205-4215. <http://www.ncbi.nlm.nih.gov/pubmed/19656848> (Not in File)

Zhao, S. L., Hong, J., Xie, Z. Q., Tang, J. T., Su, W. Y., Du, W., Chen, Y. X., Lu, R., Sun, D. F., & Fang, J. Y. (2011). TRAPPC4-ERK2 interaction activates ERK1/2, modulates its nuclear localization and regulates proliferation and apoptosis of colorectal cancer cells. *PLoS One*, 6(8), e23262. <https://doi.org/10.1371/journal.pone.0023262>

Zong, M., Wu, X. G., Chan, C. W., Choi, M. Y., Chan, H. C., Tanner, J. A., & Yu, S. (2011). The Adaptor Function of TRAPPC2 in Mammalian TRAPPs Explains TRAPPC2-Associated SEDT and TRAPPC9-Associated Congenital Intellectual Disability. *PLoS One.*, 6(8), e23350. <http://www.ncbi.nlm.nih.gov/pubmed/21858081> (Not in File)

Zykaj, E., Abboud, C., Asadi, P., Warsame, S., Almousa, H., Milev, M. P., Greco, B. M., Lopez-Sanchez, M., Bratkovic, D., Kachroo, A. H., Perez-Jurado, L. A., & Sacher, M. (2024). A Humanized Yeast Model for Studying TRAPP Complex Mutations; Proof-of-Concept Using Variants from an Individual with a TRAPPC1-Associated Neurodevelopmental Syndrome. *Cells*, 13(17). <https://doi.org/10.3390/cells13171457>